



LA GRANT
1N-84-CR
312553
P-86

Modelling and Performance Analysis of Four and Eight Element TCAS

K.S. Sampath, R.G. Rojas and W.D. Burnside

The Ohio State University
ElectroScience Laboratory

Department of Electrical Engineering
Columbus, Ohio 43212

Technical Report 716199-15
Grant No. NSG 1498
April 1990

National Aeronautics and Space Administration
Langley Research Center
Hampton, VA 23665

(NASA-CR-187414) MODELLING AND PERFORMANCE
ANALYSIS OF FOUR AND EIGHT ELEMENT TCAS
Semiannual Report, Sep. 1989 - Mar. 1990
(Ohio State Univ.) 86 p

CSCL 176

N91-13428

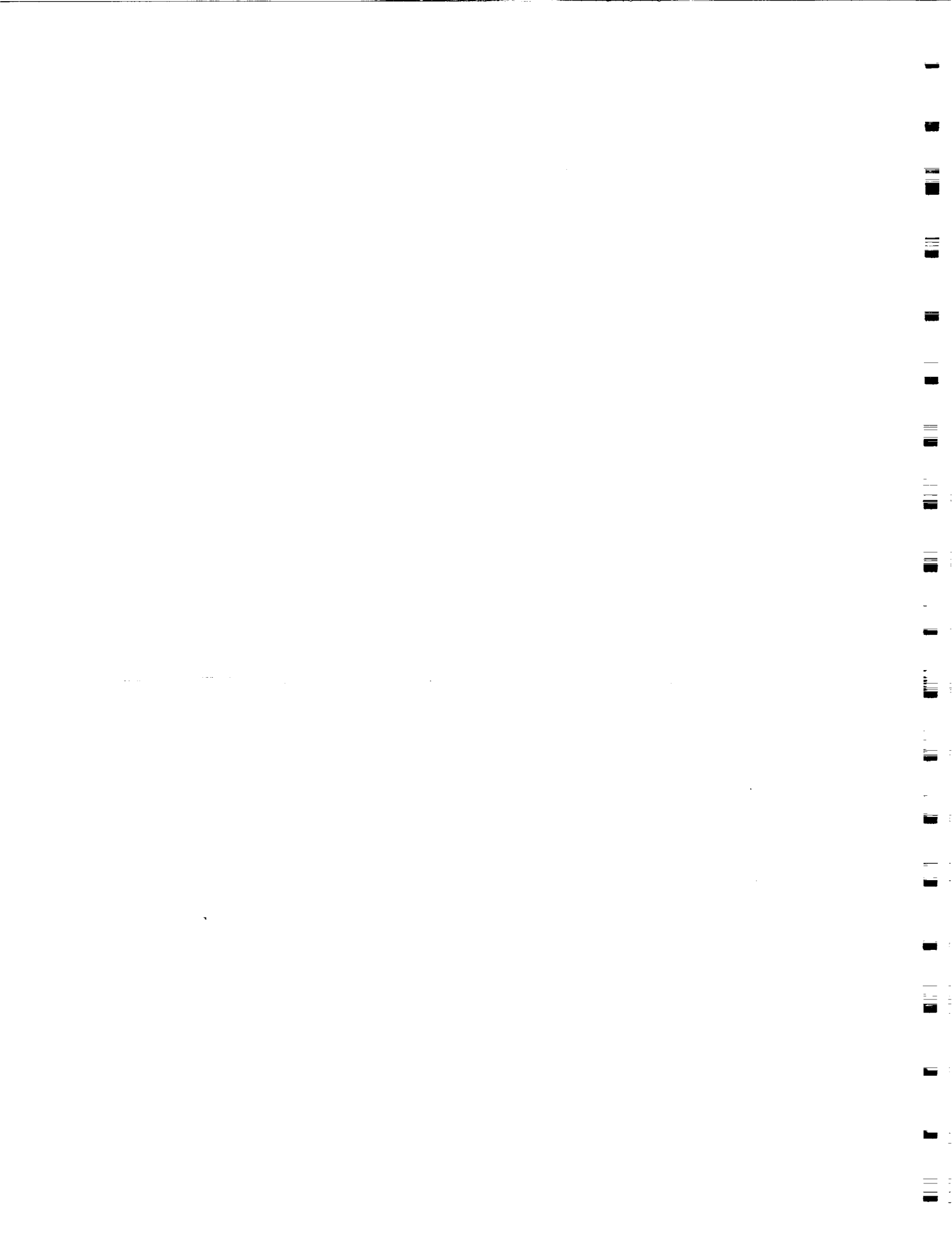
Unclas

63/04 0312553

NOTICES

When Government drawings, specifications, or other data are used for any purpose other than in connection with a definitely related Government procurement operation, the United States Government thereby incurs no responsibility nor any obligation whatsoever, and the fact that the Government may have formulated, furnished, or in any way supplied the said drawings, specifications, or other data, is not to be regarded by implication or otherwise as in any manner licensing the holder or any other person or corporation, or conveying any rights or permission to manufacture, use, or sell any patented invention that may in any way be related thereto.

REPORT DOCUMENTATION PAGE	1. REPORT NO.	2.	3. Recipient's Accession No.
4. Title and Subtitle Modelling and Performance Analysis of Four and Eight Element TCAS			5. Report Date April 1990
7. Author(s) K.S. Sampath, R.G. Rojas and W.D. Burnside			6.
9. Performing Organization Name and Address The Ohio State University ElectroScience Laboratory 1320 Kinnear Road Columbus, OH 43212			8. Performing Org. Rept. No. 716199-15
12. Sponsoring Organization Name and Address National Aeronautics and Space Administration Langley Research Center Hampton, VA 23665			10. Project/Task/Work Unit No.
			11. Contract(C) or Grant(G) No. (C) (G) NSG-1408
			13. Report Type/Period Covered Technical Report
15. Supplementary Notes			14.
16. Abstract (Limit: 200 words) This semi-annual report describes the work performed during the period September 1989-March 1990. It consists of two main sections; the first section describes the effect of the engines of the Boeing 737-200 on the performance of a bottom mounted eight-element TCAS. The second part in this report deals exclusively with a four element TCAS antenna. The model obtained to simulate the four element TCAS and new algorithms developed for studying its performance are described. The effect of location on its performance when mounted on top of a Boeing 737-200 operating at 1060 MHz is discussed. It is found that the four element TCAS generally does not perform as well as the 8 element TCAS III.			
17. Document Analysis a. Descriptors TCAS AIRCRAFT UTD b. Identifiers/Open-Ended Terms c. COSATI Field/Group			
18. Availability Statement A. Approved for public release; Distribution is unlimited.		19. Security Class (This Report) Unclassified	21. No. of Pages 86
		20. Security Class (This Page) Unclassified	22. Price



Contents

1	Introduction	1
2	Performance of Bottom Mounted TCAS III	4
2.1	Introduction	4
2.2	Aircraft and Antenna Models	4
2.2.1	Model of Aircraft	4
2.2.2	Model of TCAS	5
2.3	Error Curves	8
2.4	Results and Discussion	9
3	Four Element TCAS Studies	26
3.1	Introduction	26
3.2	Model of TCAS	27
3.3	Simulation Algorithm for TCAS	37
3.4	Results and Discussion	42
	Bibliography	67
A	Statistics of Error Curves for 4 Element TCAS	69
A.1	Location: TA	70
A.1.1	Elevation: 20°	70
A.1.2	Elevation: 10°	70
A.1.3	Elevation: 0°	70
A.1.4	Elevation: -10°	71
A.2	Location: TC	71
A.2.1	Elevation: 20°	71
A.2.2	Elevation: 10°	71

A.2.3	Elevation: 0°	71
A.2.4	Elevation: -10°	72
A.3	Location: TE	72
A.3.1	Elevation: 20°	72
A.3.2	Elevation: 10°	72
A.3.3	Elevation: 0°	72
A.3.4	Elevation: -10°	73
B	Statistics of Error Curves for 8 Element TCAS III	74
B.1	Location: TA	74
B.1.1	Elevation: 20°	74
B.1.2	Elevation: 10°	75
B.1.3	Elevation: 0°	75
B.1.4	Elevation: -10°	75
B.2	Location: TC	75
B.2.1	Elevation: 20°	75
B.2.2	Elevation: 10°	76
B.2.3	Elevation: 0°	76
B.2.4	Elevation: -10°	76
B.3	Location: TE	76
B.3.1	Elevation: 20°	76
B.3.2	Elevation: 10°	77
B.3.3	Elevation: 0°	77
B.3.4	Elevation: -10°	77

List of Figures

2.1	Model of Boeing 737-200 that includes engines for a bottom mounted TCAS III.	6
2.2	Two element model of TCAS III.	7
2.3	Error curve for TCAS III at BA about 88" from nose at -10° . No engines in the model.	11
2.4	Error curve for TCAS III at BA about 88" from nose at 0° . No engines in the model.	12
2.5	Error curve for TCAS III at BA about 88" from nose at $+10^\circ$. No engines in the model.	13
2.6	Error curve for TCAS III at BA about 88" from nose at -10° . Engines included in model. Note the high frequency oscillations.	14
2.7	Error curve for TCAS III at BA about 88" from nose at 0° . Engines included in model.	15
2.8	Error curve for TCAS III at BA about 88" from nose at $+10^\circ$. Engines included in model.	16
2.9	Error curve for TCAS III at BB about 378" from nose at -10° . No engines in the model.	17
2.10	Error curve for TCAS III at BB about 378" from nose at 0° . No engines in the model.	18
2.11	Error curve for TCAS III at BB about 378" from nose at $+10^\circ$. No engines in the model.	19
2.12	Error curve for TCAS III at BB about 378" from nose at -10° . Engines included in model.	20
2.13	Error curve for TCAS III at BB about 378" from nose at 0° . Engines included in model.	21
2.14	Error curve for TCAS III at BB about 378" from nose at $+10^\circ$. Engines included in model.	22

2.15	Error curve for TCAS III at BB about 378" from nose at -10° . Engines included in model, but not the stabilizers.	23
2.16	Error curve for TCAS III at BB about 378" from nose at 0° . Engines included in model, but not the stabilizers.	24
2.17	Error curve for TCAS III at BB about 378" from nose at $+10^\circ$. Engines included in model, but not the stabilizers.	25
3.1	Desired antenna pattern for TCAS, supplied by sponsor.	27
3.2	Geometry of the 4 element TCAS model.	28
3.3	Antenna patterns for model where $a = 2.25'', 2.31''$	31
3.4	Antenna patterns for model where $a = 2.35'', 2.4''$	32
3.5	Normalized antenna azimuth patterns for length of element $l = \lambda/10, \lambda/6, \lambda/5, \lambda/4$ for radius of array $a = 2.31''$	33
3.6	Variation of azimuth pattern at elevations $20, 10^\circ$ for TCAS model with $a = 2.31'', l = 2.78''$	34
3.7	Variation of azimuth pattern at elevations $0, -15^\circ$ for TCAS model with $a = 2.31'', l = 2.78''$	35
3.8	Actual patterns of TCAS model on Boeing 737-200 fuselage at location TC.	36
3.9	Creation of receiver beams and the lookup curve.	40
3.10	Calculation of bearing error.	41
3.11	Model of Boeing 737-200 for a top mounted TCAS antenna.	52
3.12	Explanation for discontinuities in the error curve. Data corresponds to location TC about 378" from nose, at 20° elevation.	53
3.13	Explanation for jumps in the error curve for 4 element TCAS. Data corresponds to location TC.	54
3.14	Error curve for 8 (top) and 4 (bottom) element TCAS at TA about 618.6" from nose at $+20^\circ$	55
3.15	Error curve for 8 (top) and 4 (bottom) element TCAS at TA about 618.6" from nose at $+10^\circ$	56
3.16	Error curve for 8 (top) and 4 (bottom) element TCAS at TA about 618.6" from nose at 0°	57
3.17	Error curve for 8 (top) and 4 (bottom) element TCAS at TA about 618.6" from nose at -10°	58
3.18	Error curve for 8 (top) and 4 (bottom) element TCAS at TC about 378.6" from nose at $+20^\circ$	59

3.19	Error curve for 8 (top) and 4 (bottom) element TCAS at TC about 378.6" from nose at +10°.	60
3.20	Error curve for 8 (top) and 4 (bottom) element TCAS at TC about 378.6" from nose at 0°.	61
3.21	Error curve for 8 (top) and 4 (bottom) element TCAS at TC about 378.6" from nose at -10°.	62
3.22	Error curve for 8 (top) and 4 (bottom) element TCAS at TE about 138.6" from nose at +20°.	63
3.23	Error curve for 8 (top) and 4 (bottom) element TCAS at TE about 138.6" from nose at +10°.	64
3.24	Error curve for 8 (top) and 4 (bottom) element TCAS at TE about 138.6" from nose at 0°.	65
3.25	Error curve for 8 (top) and 4 (bottom) element TCAS at TE about 138.6" from nose at -10°.	66

List of Tables

2.1	Locations of TCAS on bottom of Boeing 737-200.	5
3.1	Variation of radiation pattern of TCAS antenna model on a ground plane with increasing radius ($f = 1060$ MHz).	35
3.2	Parameters of beam pointing at 0° at various locations on Boeing 737-200 fuselage for $a = 2.31''$ and $l_{monopole} = 2.78''$	37
3.3	Reference beams for the TCAS under ideal conditions.	39
3.4	Location of intruder from received signals under ideal conditions.	39
3.5	Locations of TCAS on top of Boeing 737-200.	43
3.6	Comparison of TCAS error curves for location TC in the nose quadrant at 10° and 0° elevations.	48
3.7	Comparison of TCAS error curves for location TC in the side quadrants at 10° and 0° elevations.	48
3.8	Comparison of TCAS error curves for location TC in the tail quadrant at 10° and 0° elevations.	49
3.9	Comparison of TCAS error curves for location TC in the nose quadrant at 20° and -10° elevations.	49
3.10	Comparison of TCAS error curves for location TC in the side quadrants at 20° and -10° elevations.	49
3.11	Comparison of TCAS error curves for location TC in the tail quadrant at 20° and -10° elevations.	50
A.1	Definition of sectors for computation of statistics for the error curves for top mounted antennas.	69

Chapter 1

Introduction

The study reported here was performed during the period September 1989 through March 1990. It is a continuation of previous studies on the performance of a TCAS antenna mounted on the fuselage of an aircraft. In all previous studies and in Chapter 2 of this report, the TCAS antenna is a 8-element circular monopulse array designed by Bendix [2]. The details of this system are reported elsewhere [1]-[5] and will not be repeated here, except for its more important features. Thus, in Chapter 2, only the performance of this 8-element TCAS monopulse antenna mounted on the bottom of a Boeing 737-200 aircraft is discussed. One of the goals of this study was to see the effect of the engines on the performance of the TCAS system. As expected, it is shown that the TCAS monopulse system is adversely affected by the engines of the aircraft when it is mounted on the bottom of the fuselage. It is also shown that the effect of the engines can be reduced by moving the antenna location away from the engines towards the nose of the aircraft.

Recall that the 8-element TCAS antenna transmits and receives sum

and difference beams at 1030 MHz and 1090 MHz, respectively. The element excitations are generated with a beam forming network which uses a Butler matrix and the beams are electronically steered by means of phase shifters [2]. The bearing of an intruder with respect to the TCAS equipped aircraft is determined by a monopulse angle measurement technique. For this purpose, a monopulse characteristic curve is generated by appropriately combining the sum and difference beams [3].

Although in previous studies [5] it has been shown that this monopulse system performs very well, its construction is complicated and costly. Thus, there is a need for an alternative angle measurement system which is simpler and less expensive to build. Thus, the second part of this report, namely, Chapter 3, describes a four-element TCAS amplitude comparison measurement system.

In this system, the four element circular array transmits a beam in one of four selectable directions. The array is mounted on the aircraft and aligned in such a way that the beams are directed in the directions of 0° , 90° , 180° and 270° of relative bearing. The beams must have a 3-dB beamwidth of $90^\circ \pm 10^\circ$ for all elevation angles between $+20^\circ$ and -15° , and as in the monopulse system, these are transmitted at 1030 MHz. In contrast to the monopulse system, this antenna array receives signals omnidirectionally at 1090 MHz. By omnidirectionally, it is meant that all of the four beams mentioned above are used to receive the incoming signals where each of these beams is connected to a different receiver. The magnitude of the four received signals are then compared and the difference of the largest two is taken. This result is then compared against a calibration or lookup table

to determine the bearing of the aircraft under observation. This amplitude comparison scheme is simpler to build than the monopulse system and, as shown in this report, appears to perform fairly well.

Chapter 2

Performance of Bottom Mounted TCAS III

2.1 Introduction

This chapter describes the effect of the engines of the Boeing 737-200 on the performance of a bottom mounted eight element TCAS III antenna. The performance of this antenna at two locations on the bottom of this aircraft are studied in detail where each engine was modelled by a set of flat plates making up a box. As expected, it is found that the performance of the system is degraded substantially when the antenna is close to the midsection of the aircraft because of the engines.

2.2 Aircraft and Antenna Models

2.2.1 Model of Aircraft

The fuselage was modelled by a composite ellipsoid, whereas, the wings and the horizontal stabilizer were modelled by flat plates. It is noted that

Antenna Location	Z coordinate (inches)	Distance from nose (inches)
BA	-144.6	87.6
BB	70.0	378.6

Table 2.1: Locations of TCAS on bottom of Boeing 737-200.

sometimes for a bottom mounted antenna, as it is the case here, it is not necessary to include the vertical stabilizer because it is in the shadow region of the antenna and the antenna location is far away from this particular stabilizer. Of course, to validate this conclusion, radiation patterns were obtained with and without the vertical stabilizer and no noticeable changes in the antenna patterns were observed. As mentioned before, each engine was modelled by flat plates joined to make up a box like structure. It was found that each engine could be reasonably well approximated by a set of 4 flat plates. This is shown in Figure 2.1.

2.2.2 Model of TCAS

The eight element TCAS was modelled by the "two monopoles per actual element" model which was developed and validated earlier by [6] and is shown in Figure 2.2. This model is quite accurate in the forward half space of the aircraft and is reasonable even in the back. It is also simple enough so that not too much time is spent calculating the element patterns in the aircraft antenna code [7].

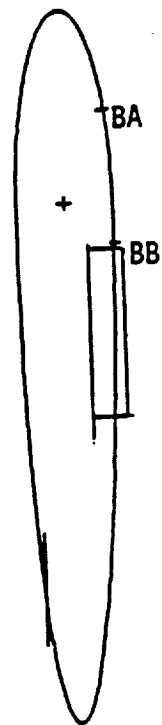
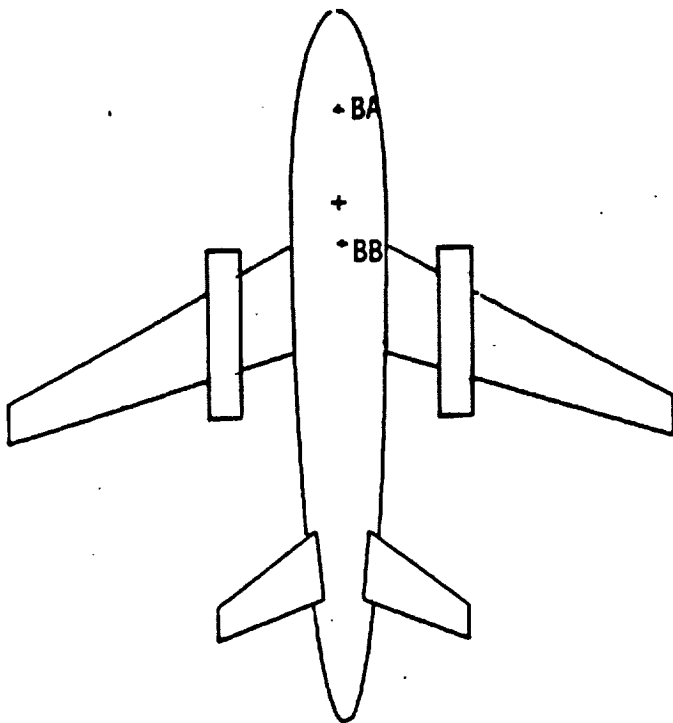
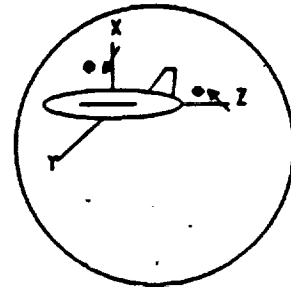
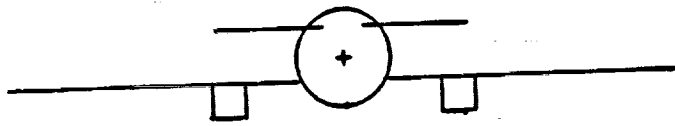


Figure 2.1: Model of Boeing 737-200 that includes engines for a bottom mounted TCAS III.

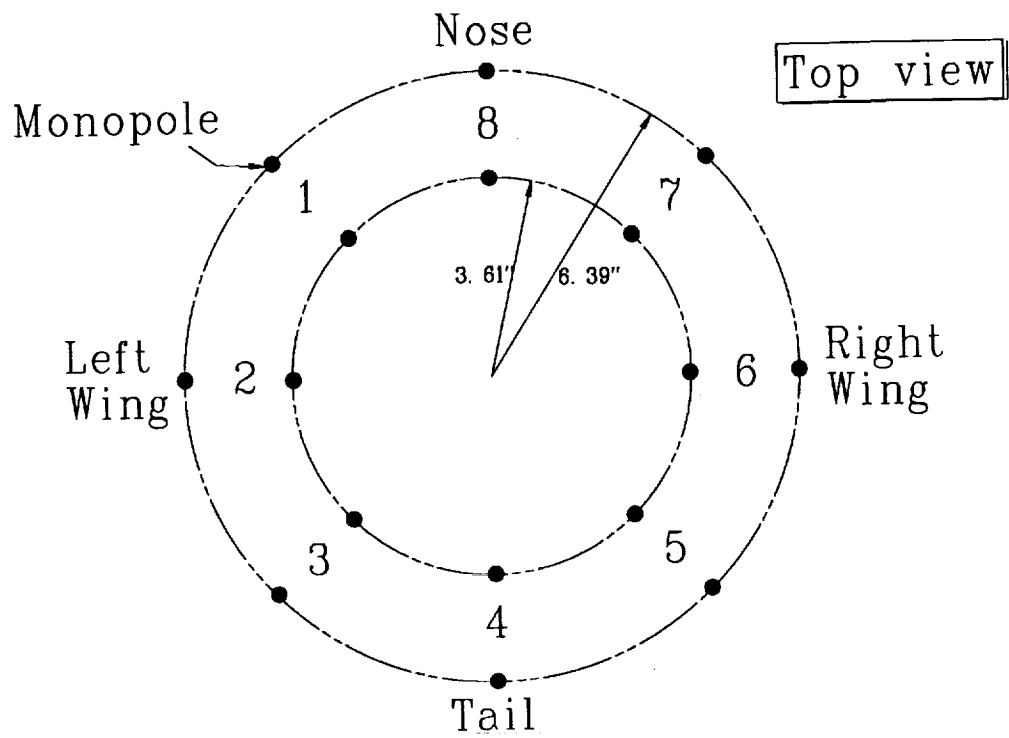


Figure 2.2: Two element model of TCAS III.

2.3 Error Curves

The element patterns for each of the "two-monopole" elements were obtained at each location of the TCAS on the fuselage. These were then added with the appropriate phase so as to get the array patterns for the sum (Σ) and difference (Δ) beams. A total of 64 such pairs were generated with each pair of sum and difference beam covering $360/64 = 5.625^\circ$ of azimuth. These were then used to create the monopulse curves. As in previous studies, two sets of monopulse curves were created; namely, the "lookup" tables, where only the fuselage is included in the model, and a set of monopulse curves where the aircraft model includes all scatterers such as the wings, engines and stabilizers. These two sets of monopulse curves were further processed to get the error curves. The actual details of this procedure can be found in [5]-[6].

In this report, error curves for a symmetrically mounted TCAS on the bottom of a Boeing 737-200 are given. The main goal of this research was to see what kind of effect the engines have on the performance of a bottom-mounted eight element TCAS antenna. As stated above, the engines are modelled with four plates that form a box. In other words, the model being used here does not have an inlet. This model will in general predict higher levels of scattering than the actual engine because the engine inlet is modelled by a flat plate which blocks off all the electromagnetic fields which enter the inlet. Therefore, the predicted bearing errors will probably be higher than the actual errors. At the present time the aircraft code being used for this study does not have the capability to accurately model

inlets. A number of solutions have been developed at the ElectroScience Laboratory to handle the scattering by inlets; however, they are not as yet implemented in the aircraft code [8]–[10].

2.4 Results and Discussion

Error curves are presented below for two antenna locations; namely, one where the antenna is closer to the nose than the engines, and a second location where the antenna is very close to the engines. For reference, error curves are also given for the two locations without including the engines in the aircraft model. The two locations are labelled BA and BB and their corresponding distance from the nose are given in Table 2.1. The first character identifies the position of the TCAS on the fuselage, B indicating a bottom mounted antenna. Error curves for each of the two locations BA and BB are given for the elevation angles of -10° , 0° , and $+10^\circ$, respectively. These curves appear in Figures 2.3–2.14.

In these curves, the header in each curve contains some useful information also. The first line of the header identifies the location of TCAS and the elevation angle. The second line gives the statistical information about the forward quadrant, ie, $-45^\circ \leq \phi \leq +45^\circ$ range. The absolute value of the maximum error in this range, average and standard deviation are given. This is also referred to as the 'nose' quadrant. The third line gives information about the location of the antenna, distance from the nose and any other relevant information about the model. The following observations can be made from these results.

First of all it is clear that the error curves are very sensitive to the elevation angle. For the two antenna locations on the bottom of the Boeing 737-200 one notices that the error decreases as one gets lower (more negative elevation). This is due to less interference from the scattering components on the aircraft as well as getting closer to the elevation angle for which the lookup table was created. Further, the curvature of the fuselage and the resultant shadowing of the antenna from the intruder above a certain elevation also tends to increase the error.

The distance of the antenna from the engines also affects the performance of the TCAS III. The performance gets worse as one moves closer to the engines. For example, in the case of the TCAS at location BB, the predicted bearing error (with the engines included) is so large as to render the system useless in a direction finding application. The location BA near the nose gives better results although the effects of engines are still observable. As expected, the errors do decrease as the elevation gets more negative because one is getting deeper into the lit region of the TCAS III and the diffraction effects are less pronounced.

One also notices that the horizontal and vertical stabilizers do not play any significant role in the characteristic. This is seen from the Figures 2.15, 2.16, and 2.17 which are virtually identical to Figures 2.12, 2.13, and 2.14 respectively. This is due to the large distance between the antenna and the stabilizers. Further, these are shadowed by the fuselage and the only rays that reach the tail are the creeping rays and some double diffracted rays. The effect of these higher order mechanisms is even smaller and are ignored.

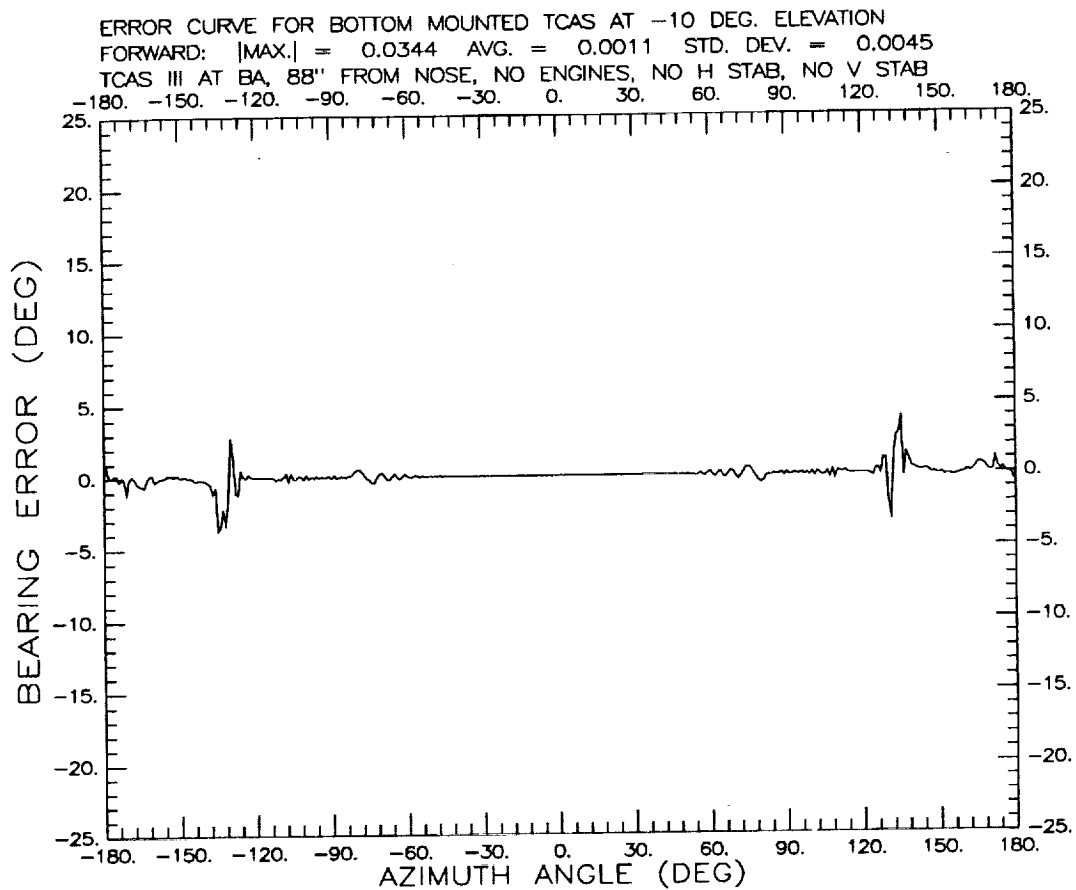


Figure 2.3: Error curve for TCAS III at BA about 88" from nose at -10° . No engines in the model.

It important to reiterate that the model of the engine is simple and is an over simplification of the real engine. Presently, there is no way to incorporate all the effects of the inlets in the aircraft code. Thus, the predicted bearing errors are probably somewhat higher than the actual bearing errors.

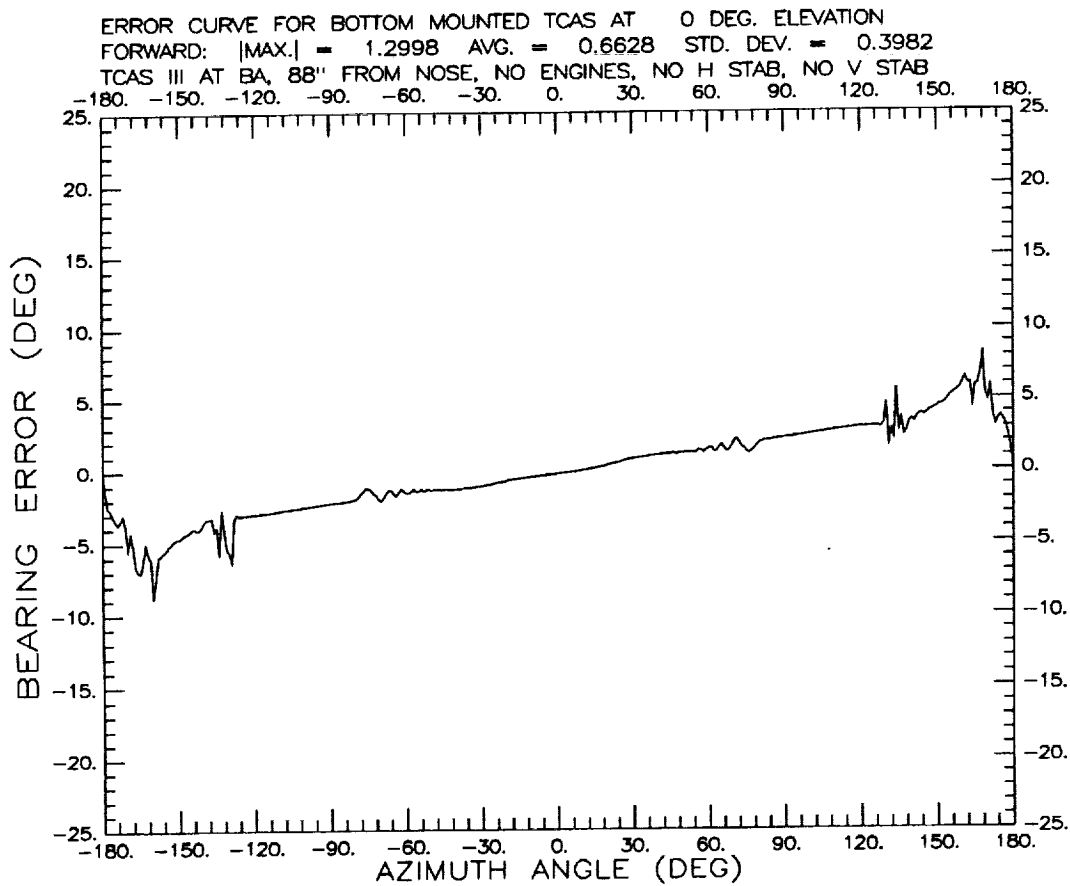


Figure 2.4: Error curve for TCAS III at BA about 88" from nose at 0°. No engines in the model.

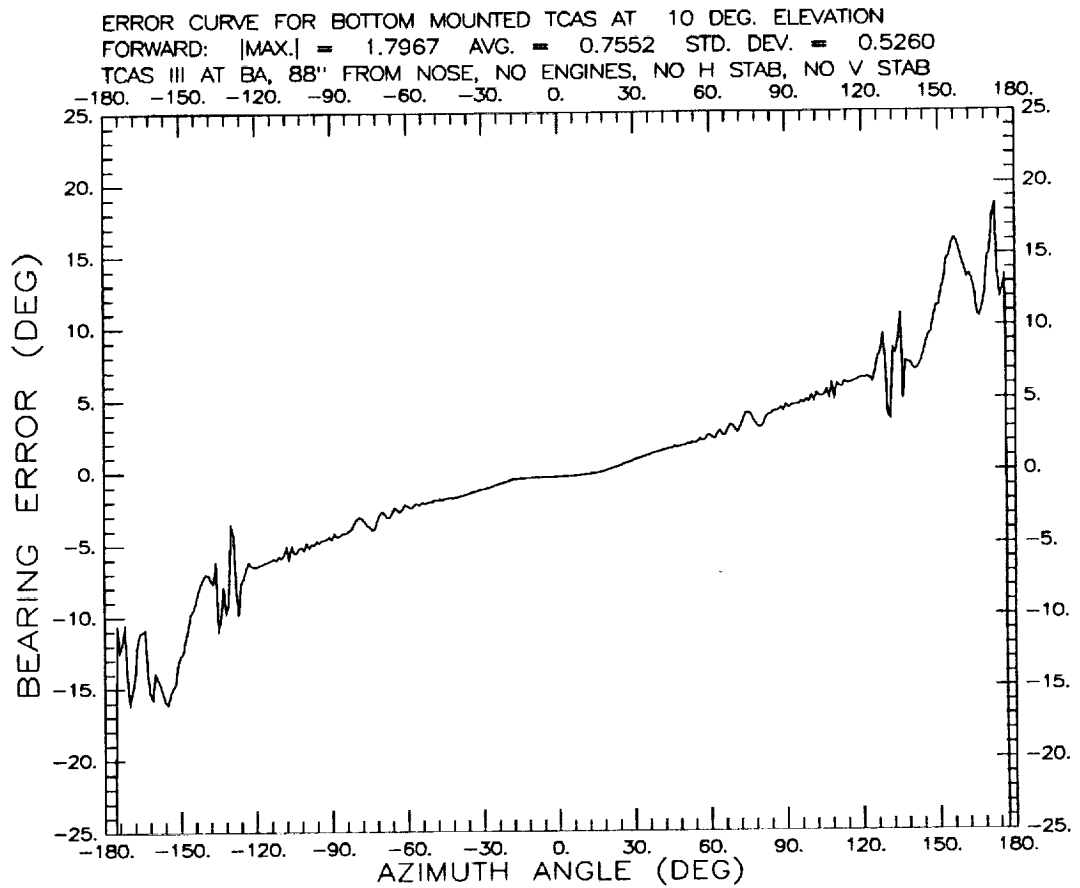


Figure 2.5: Error curve for TCAS III at BA about 88" from nose at +10°. No engines in the model.

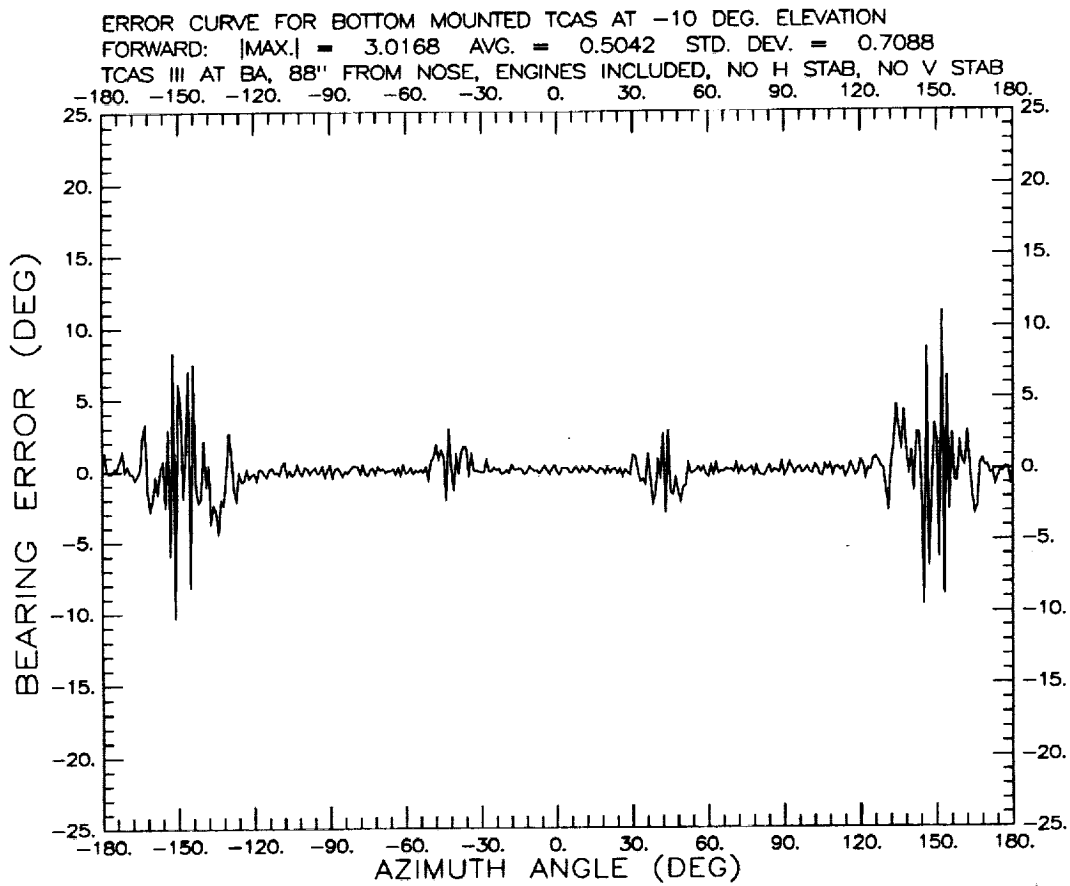


Figure 2.6: Error curve for TCAS III at BA about 88" from nose at -10° . Engines included in model. Note the high frequency oscillations.

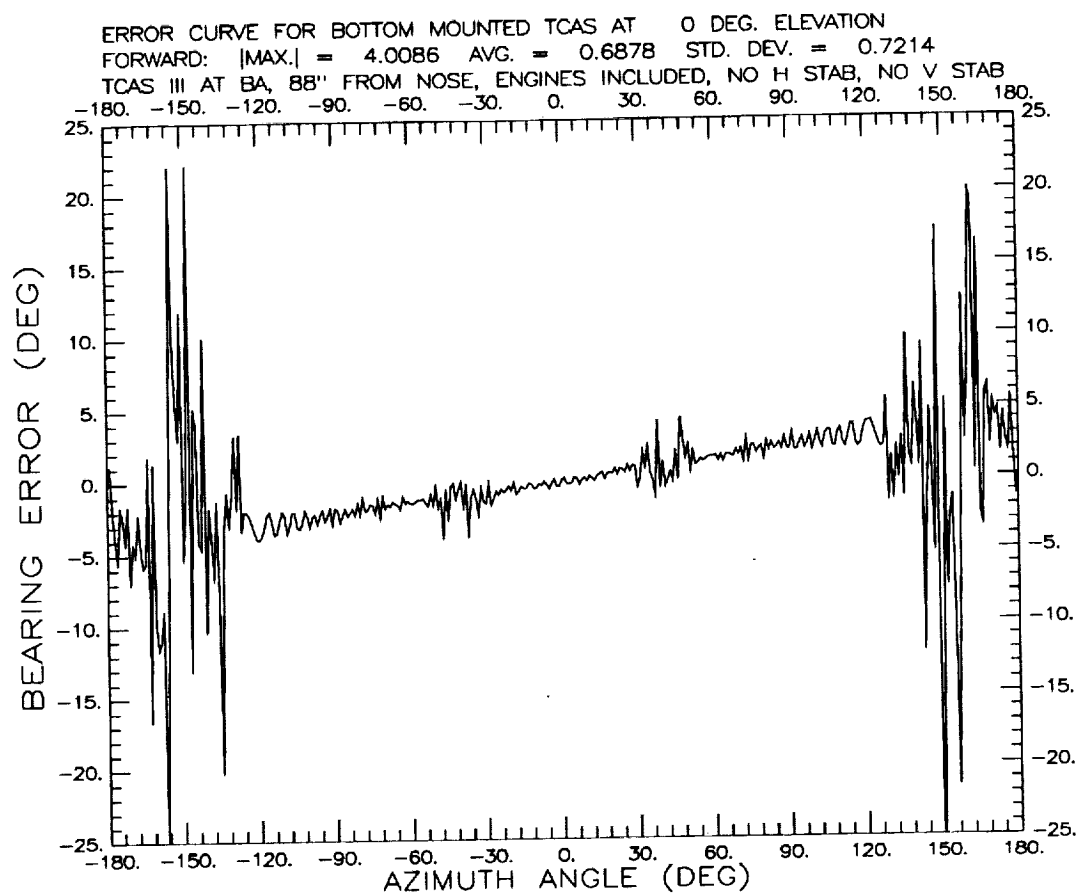


Figure 2.7: Error curve for TCAS III at BA about 88" from nose at 0°. Engines included in model.

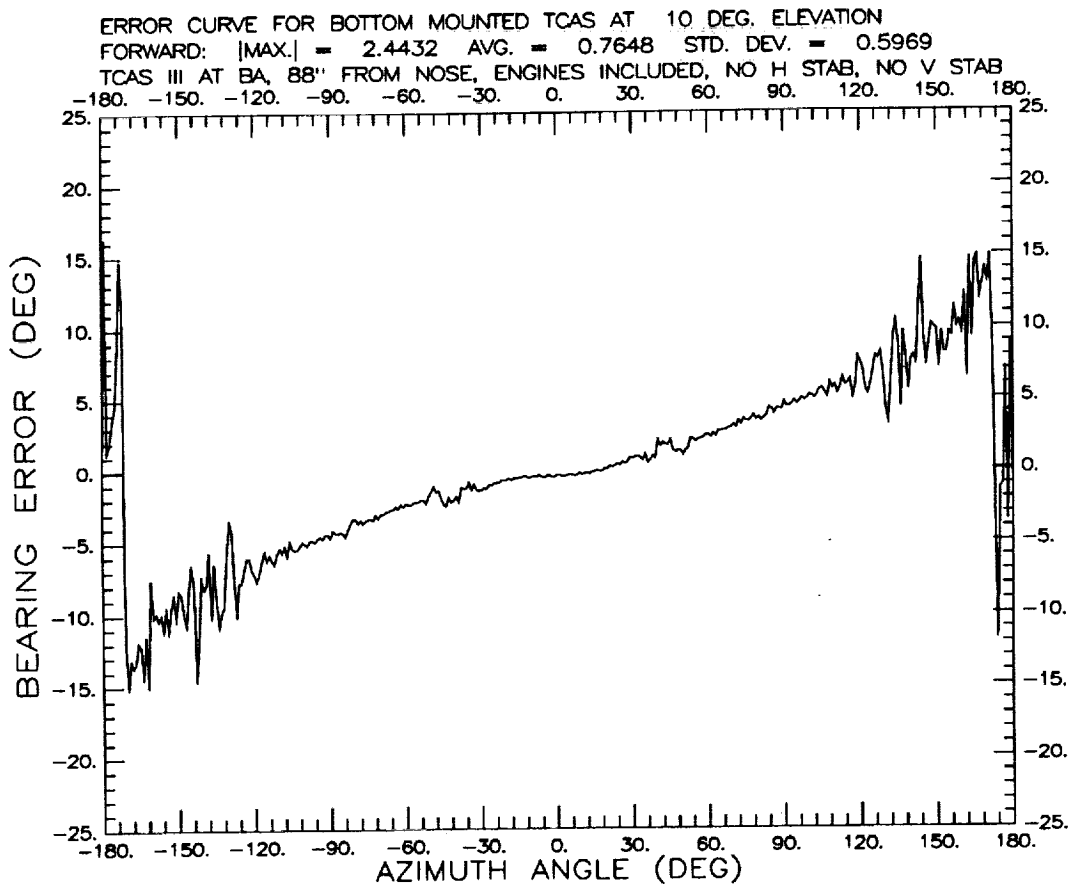


Figure 2.8: Error curve for TCAS III at BA about 88" from nose at +10°. Engines included in model.

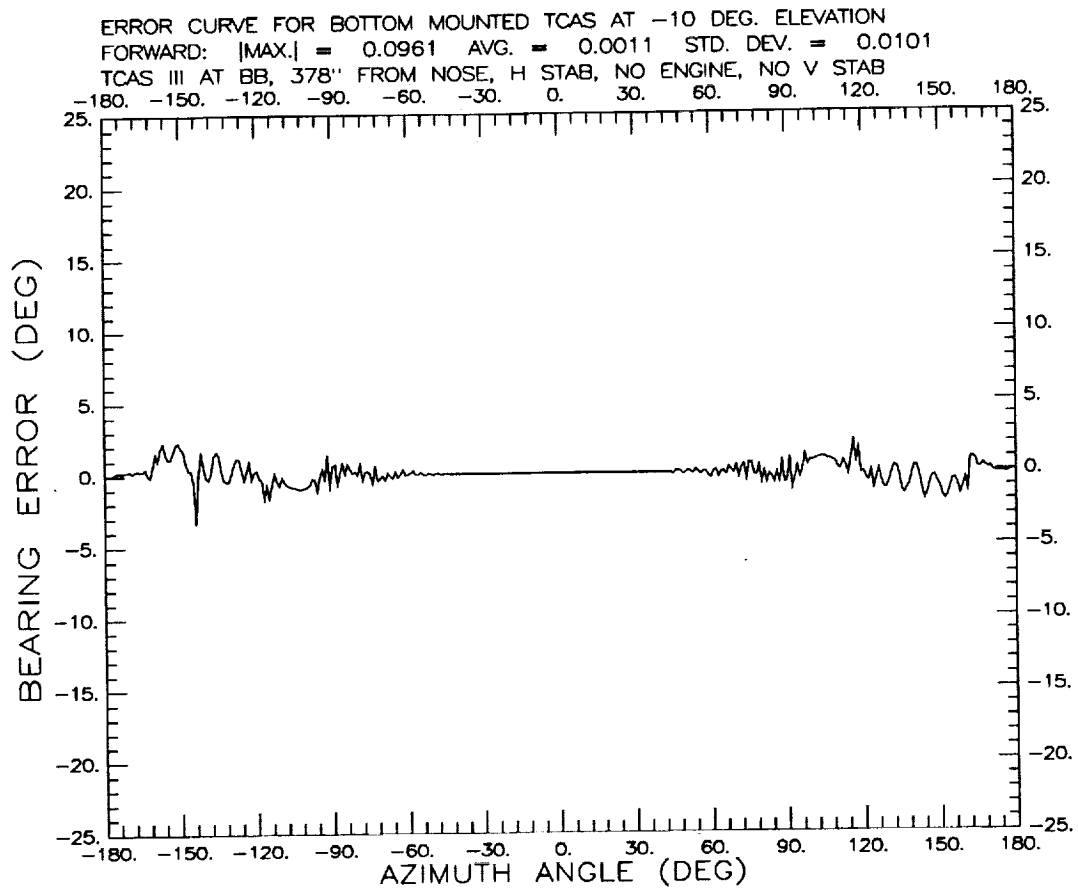


Figure 2.9: Error curve for TCAS III at BB about 378" from nose at -10° .
 No engines in the model.

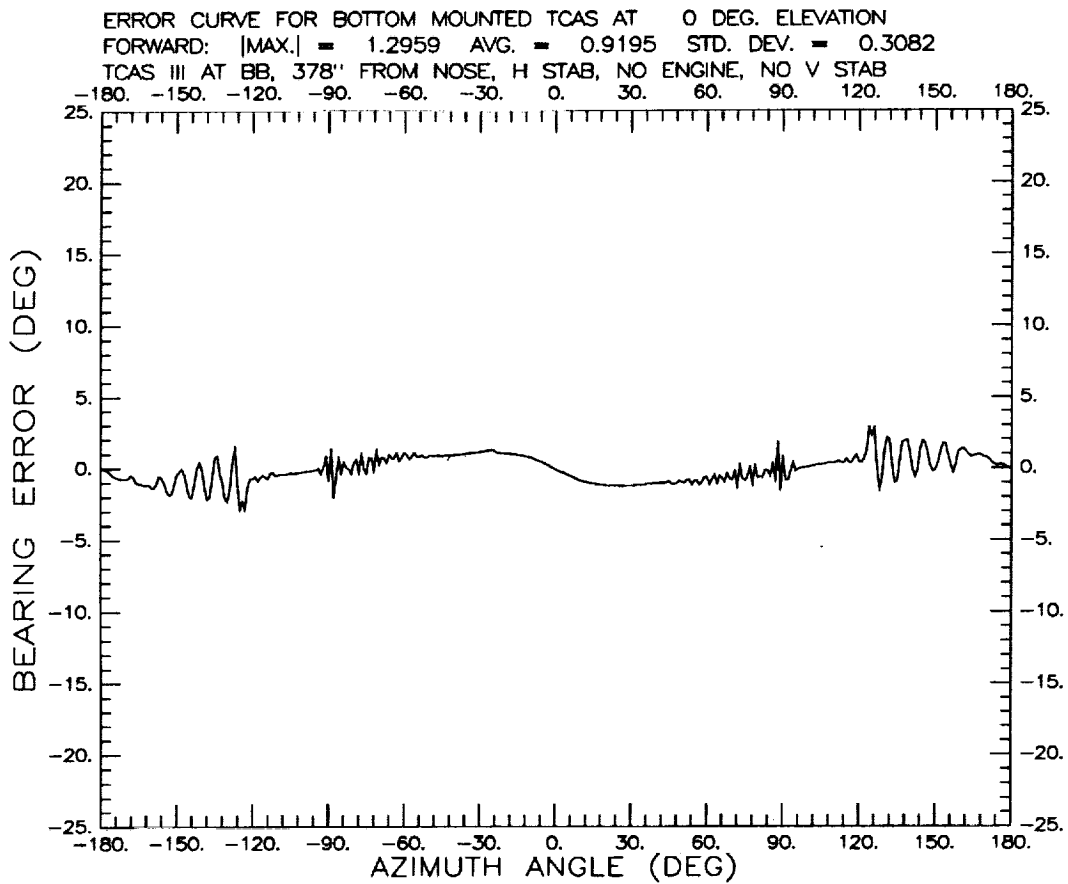


Figure 2.10: Error curve for TCAS III at BB about 378" from nose at 0°. No engines in the model.

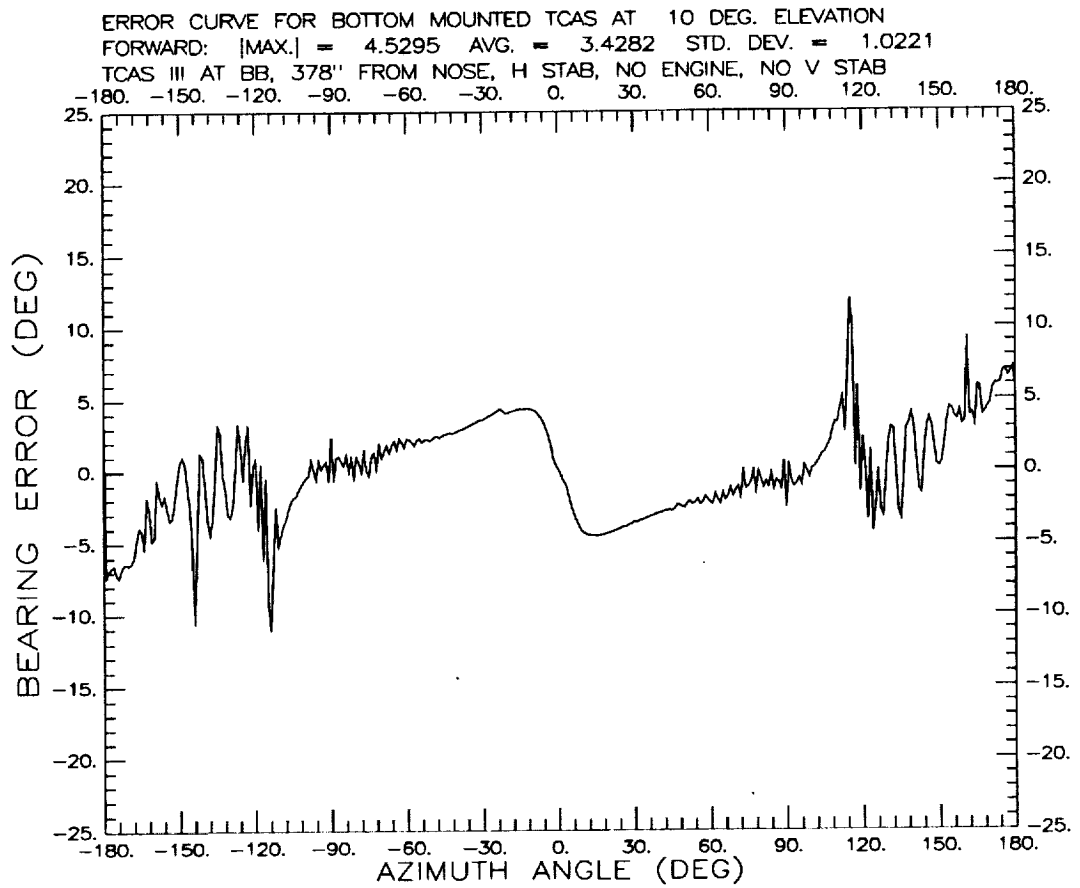


Figure 2.11: Error curve for TCAS III at BB about 378" from nose at +10°. No engines in the model.

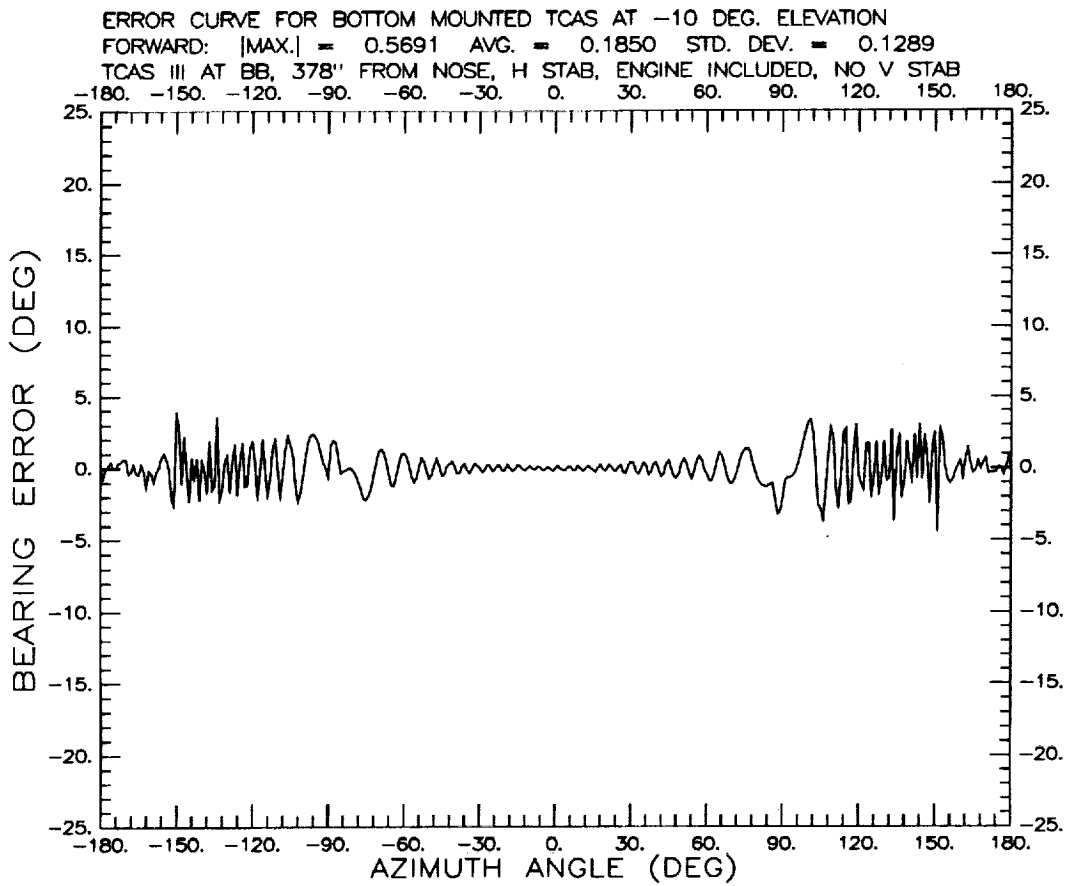


Figure 2.12: Error curve for TCAS III at BB about 378" from nose at -10°. Engines included in model.

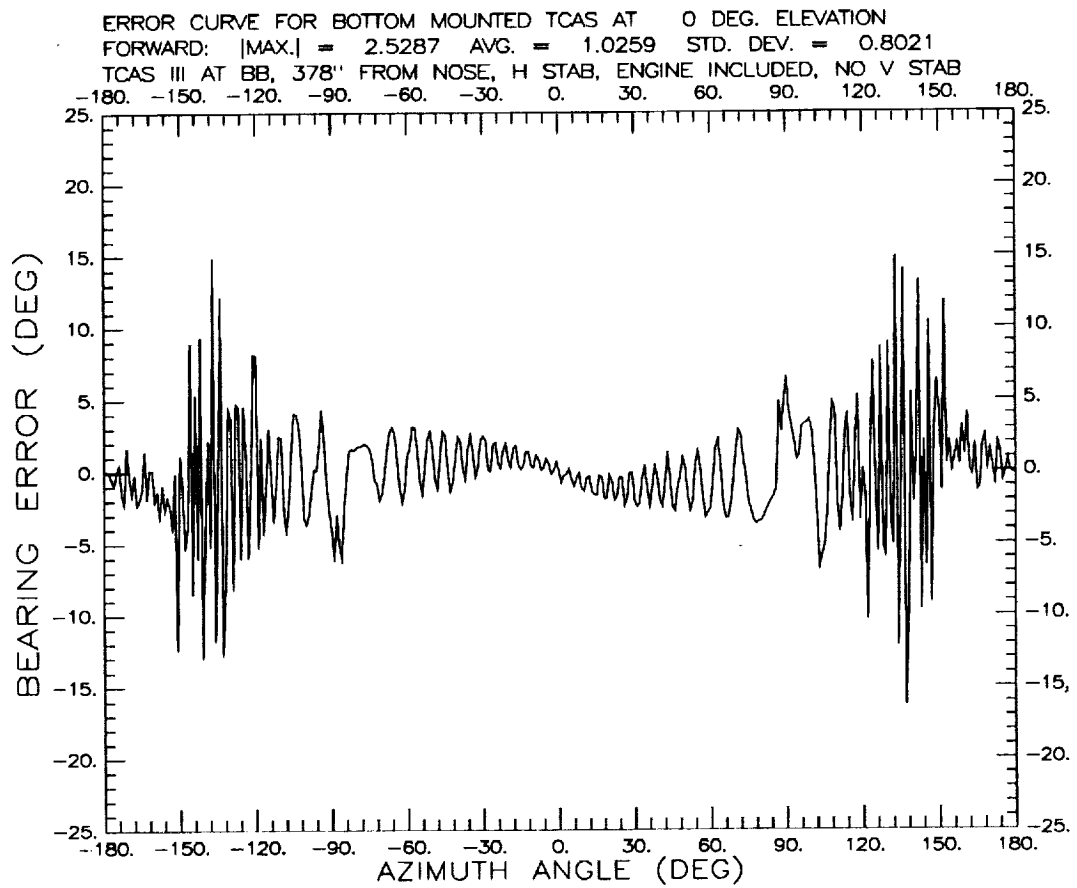


Figure 2.13: Error curve for TCAS III at BB about 378" from nose at 0°. Engines included in model.

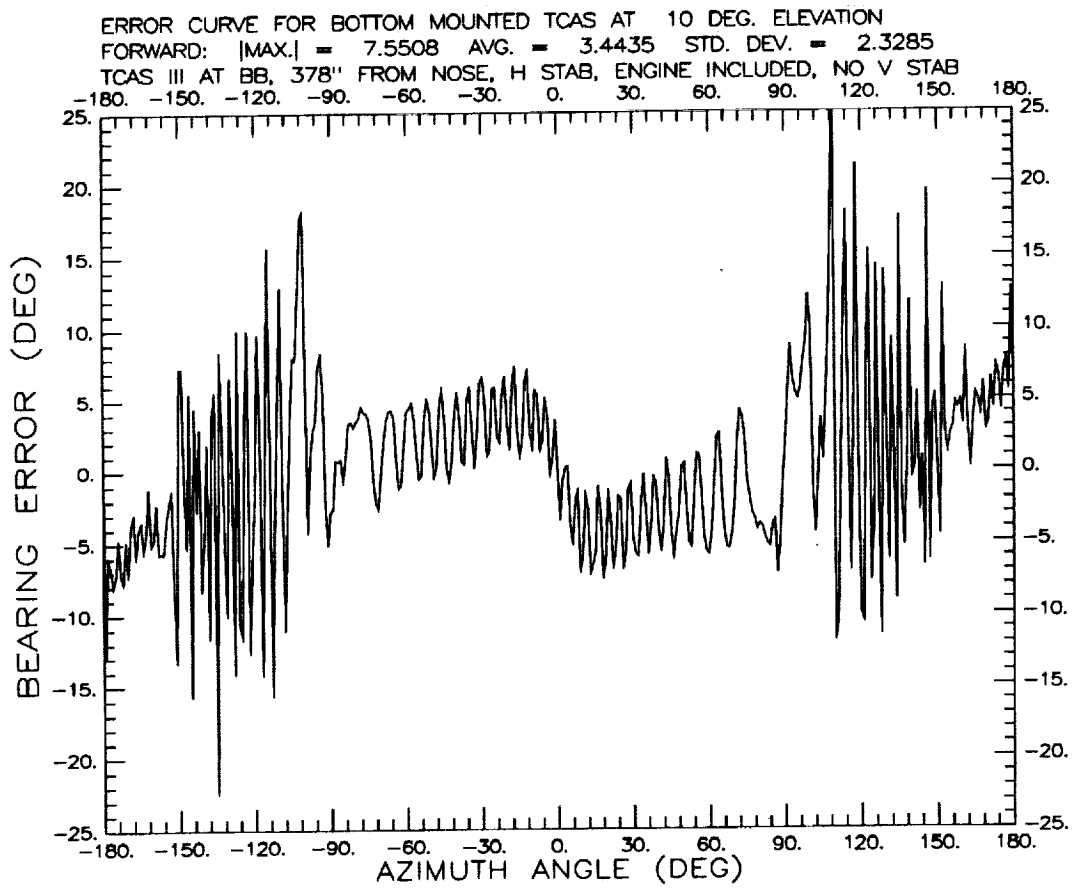


Figure 2.14: Error curve for TCAS III at BB about 378" from nose at +10°. Engines included in model.

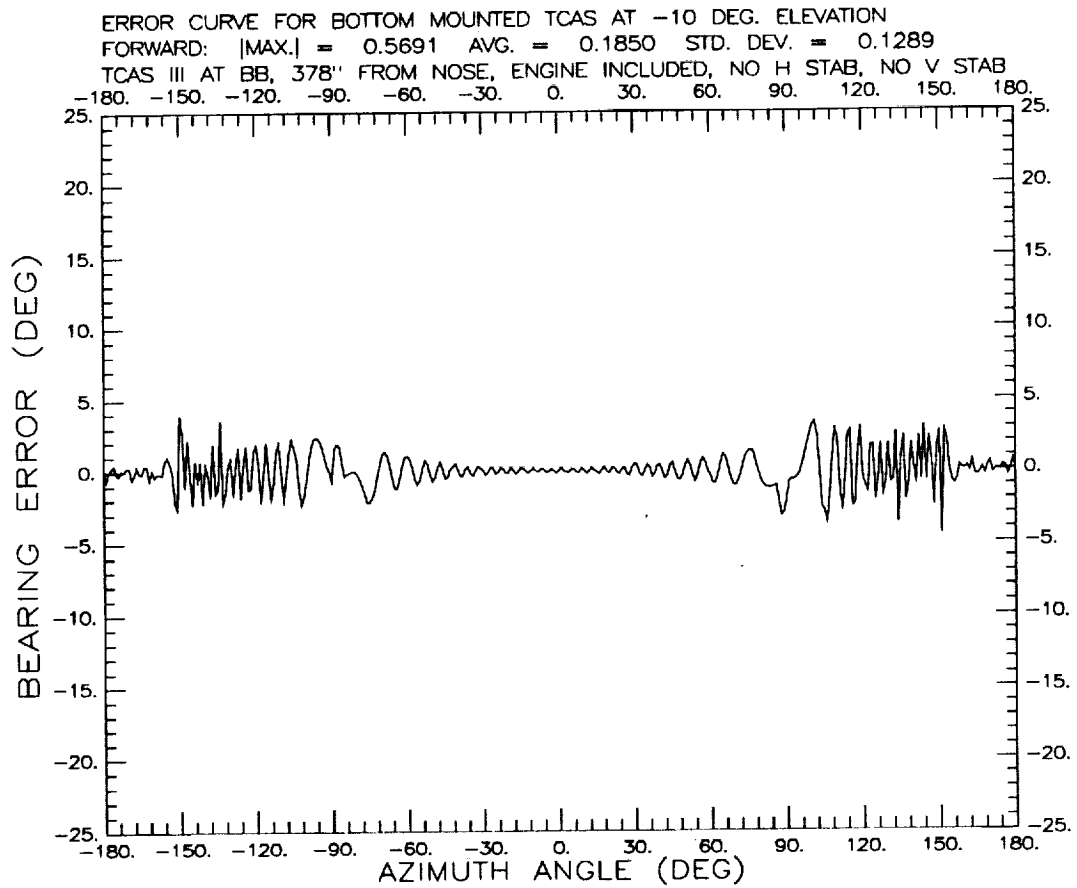


Figure 2.15: Error curve for TCAS III at BB about 378" from nose at -10° .
 Engines included in model, but not the stabilizers.

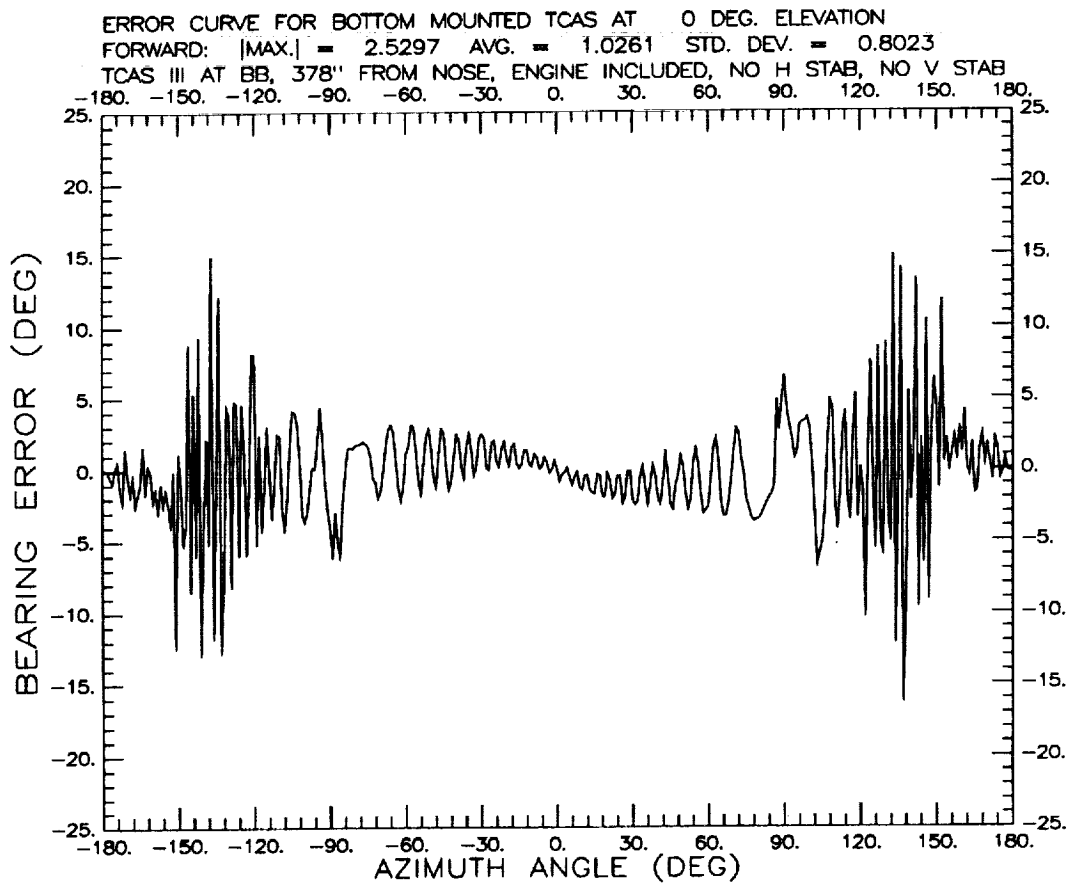


Figure 2.16: Error curve for TCAS III at BB about 378" from nose at 0°. Engines included in model, but not the stabilizers.

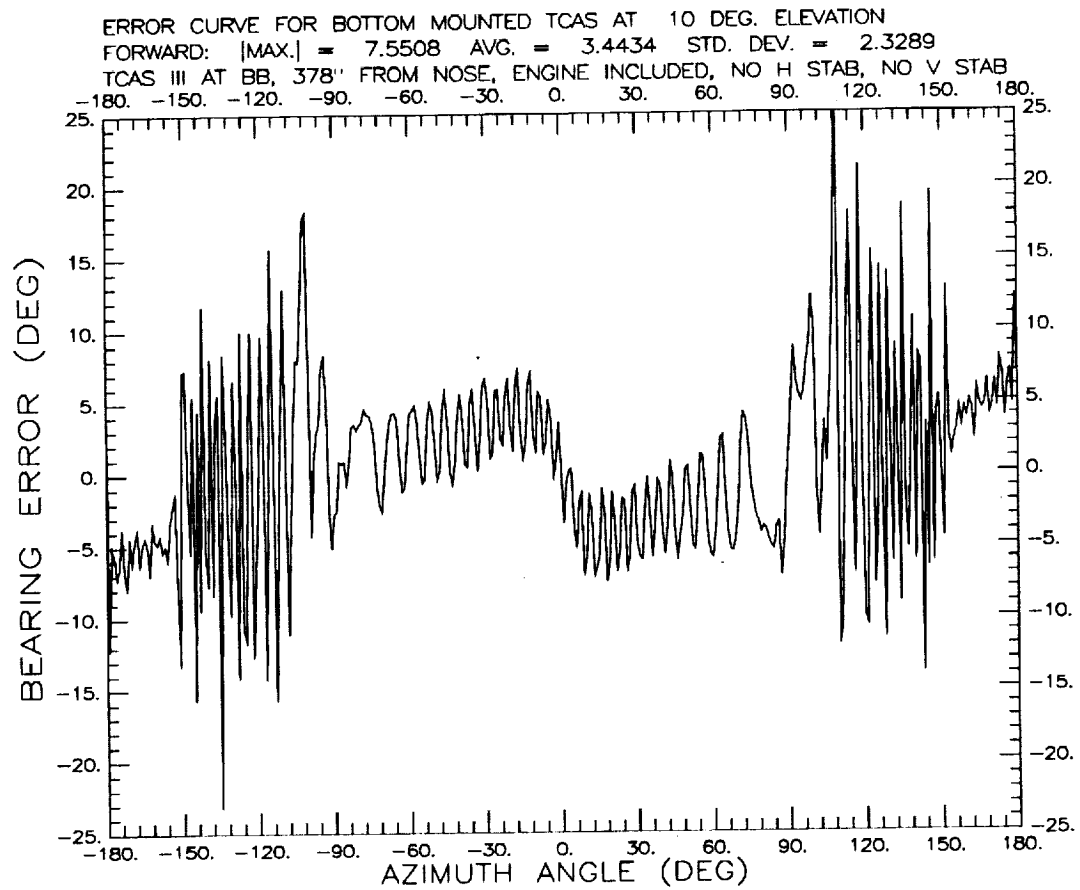


Figure 2.17: Error curve for TCAS III at BB about 378" from nose at +10°. Engines included in model, but not the stabilizers.

Chapter 3

Four Element TCAS Studies

3.1 Introduction

This chapter describes the operation of the four element TCAS. First, the antenna is modelled by four short monopoles located on a circle. The effect of varying the diameter on the pattern is discussed. A choice of antenna is made based on closeness of this approximation to the given specifications of the TCAS antenna. This is used in the aircraft antenna code [7] to obtain element patterns of individual elements. The results obtained from the aircraft code are then weighted and added to obtain the array patterns of the TCAS antenna in the four directions, ie., forward, left (port side), tail, and right (starboard side). This data is processed to get error curves for the four element TCAS. It is found that the performance is not as good as the corresponding eight element monopulse TCAS system at the same location on the same aircraft.

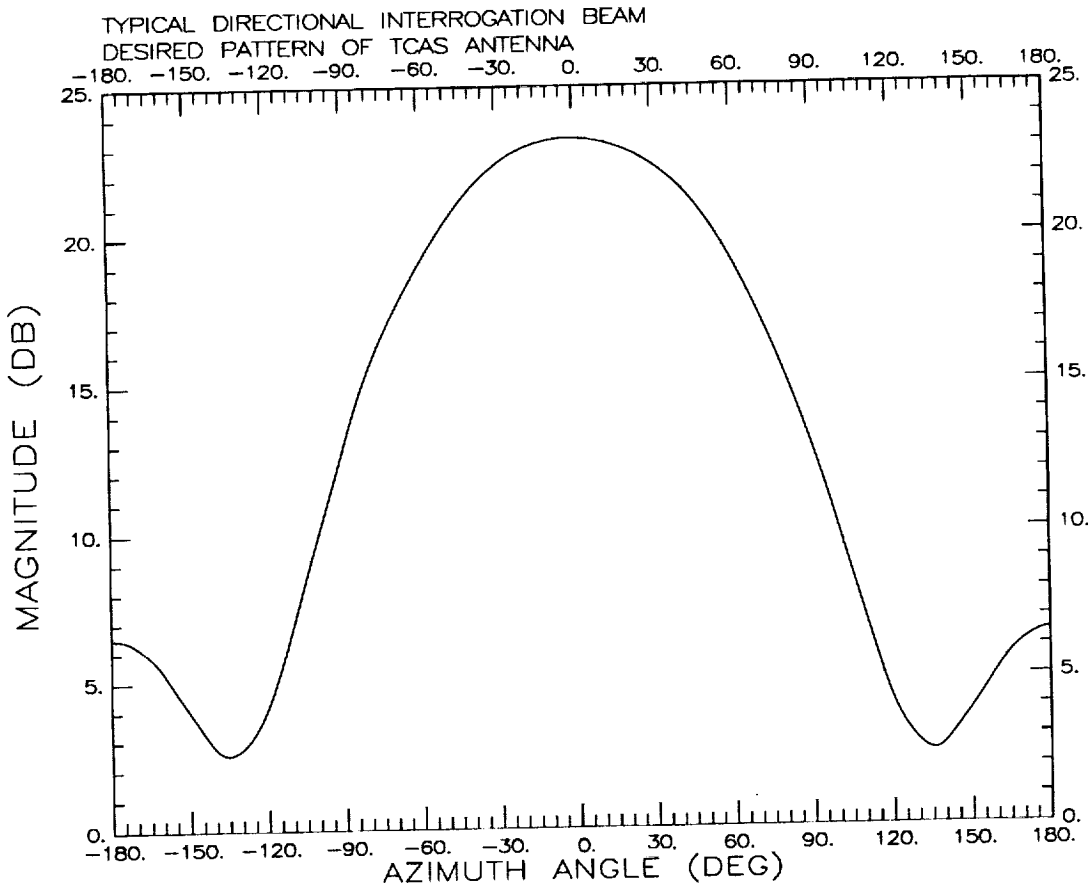


Figure 3.1: Desired antenna pattern for TCAS, supplied by sponsor.

3.2 Model of TCAS

The specifications for the TCAS require that the beam have a 3-dB beamwidth of $90 \pm 10^\circ$ and a 10-dB beamwidth of $180 \pm 10^\circ$ for all elevation angles between $+20^\circ$ and -10° . A sketch of the desired pattern is given in Figure 3.1.

The TCAS is modelled by 4 short z -directed monopoles on a flat ground plane with sinusoidal current distributions. This is shown in Figure 3.2.

Let the excitation of the individual elements be given by

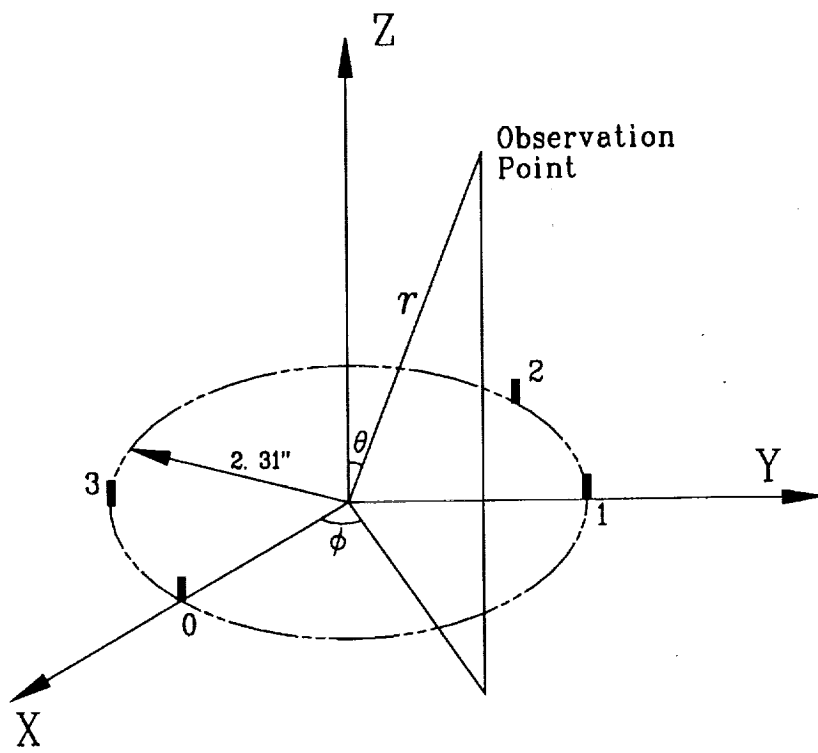


Figure 3.2: Geometry of the 4 element TCAS model.

$$I_i = A_i e^{j\alpha_i} \quad (3.1)$$

where I_i is the complex excitation, A_i is the amplitude, α_i is the phase of the i^{th} element respectively where $i = 0, 1, 2, 3$, and $j = \sqrt{-1}$. The elements are counted counterclockwise (ccw) from the X-axis as shown.

The far field antenna pattern $E_\theta(\theta, \phi)$ is the product of the element pattern ($F(r, \theta, \phi)$) and the array factor ($AF(\theta, \phi)$) such that

$$E_\theta(\theta, \phi) = F(r, \theta, \phi) \cdot AF(\theta, \phi) \quad (3.2)$$

where, the element pattern of a dipole of length l or a monopole of length $l/2$ on a ground plane with a sinusoidal current distribution can be written as [11]

$$F(r, \theta, \phi) = \frac{j\eta I_0 e^{-jkr}}{2\pi r} \left[\frac{\cos \frac{kl}{2} \cos \theta - \cos \frac{kl}{2}}{\sin \theta} \right] \quad (3.3)$$

and

$$AF(\theta, \phi) = \sum_{i=0}^3 A_i e^{j(\alpha_i + ka \sin \theta \cos(\phi - \phi_i))} \quad (3.4)$$

where, a is the radius of the array, and k is the free space wavenumber, and $k = 2\pi/\lambda$. Note that ϕ_i is the angular position of the i^{th} element with $\phi_i = i \cdot 90^\circ$, η is the impedance of free space, and (r, θ, ϕ) are the standard coordinates in a spherical coordinate system.

Since the number of elements is small (four), the amplitudes are set to a constant value $A_i = A$, and only the phase of the excitation is modified so as to get a maximum in any one of the four directions given by $\phi_j = j \cdot 90^\circ$ ($j = 0, 1, 2, 3$), corresponding to nose, left, tail, and right directions respectively. Also, to have a symmetrical horizontal pattern, the two elements

perpendicular to the axis of beam heading must have the same phase. From these requirements, for example, for a beam maximum in the direction of the nose ($\theta = \theta_0, \phi = 0^\circ$), one must have

$$\begin{aligned}\alpha_0 &= \text{arbitrary}, \\ \alpha_1 &= \alpha_0 + ka \sin \theta_0 \\ \alpha_2 &= \alpha_0 + 2ka \sin \theta_0, \text{ and} \\ \alpha_3 &= \alpha_1.\end{aligned}\tag{3.5}$$

The weights were calculated for each beam heading $\phi_j = j \cdot 90^\circ$ and $\theta_0 = 80^\circ$, because it corresponds to the elevation angle of most interest, namely 10° . These weights are then kept fixed in all further calculations.

Some resulting antenna patterns for an elevation of $+10^\circ$ are given in Figures 3.3 and 3.4 for various radii of the array. A comparison of these designs is found in Table 3.1. It is found that the pattern is sensitive to the value of ka .

Plots are also provided for the case where the radius a has been fixed at 2.31 inches and the length of the monopole is varied from 0.1λ to 0.25λ . Four antenna lengths, $l = \lambda/10, \lambda/6, \lambda/5$, and $\lambda/4$ were considered ($\lambda = 11.142''$ at 1060 MHz). This can be found in Figure 3.5 where the *normalized* antenna pattern is plotted for various lengths in the horizontal plane (elevation= 10°). The length of the antenna elements affects only the elevation plane patterns, and the effect is very small for $l < \lambda/4$. Note that all the four azimuth plane curves are virtually identical and indistinguishable. The length l cannot be chosen greater than $\lambda/4$ because of limitations of the aircraft antenna code. Thus, any length $l \leq \lambda/4$ can be chosen.

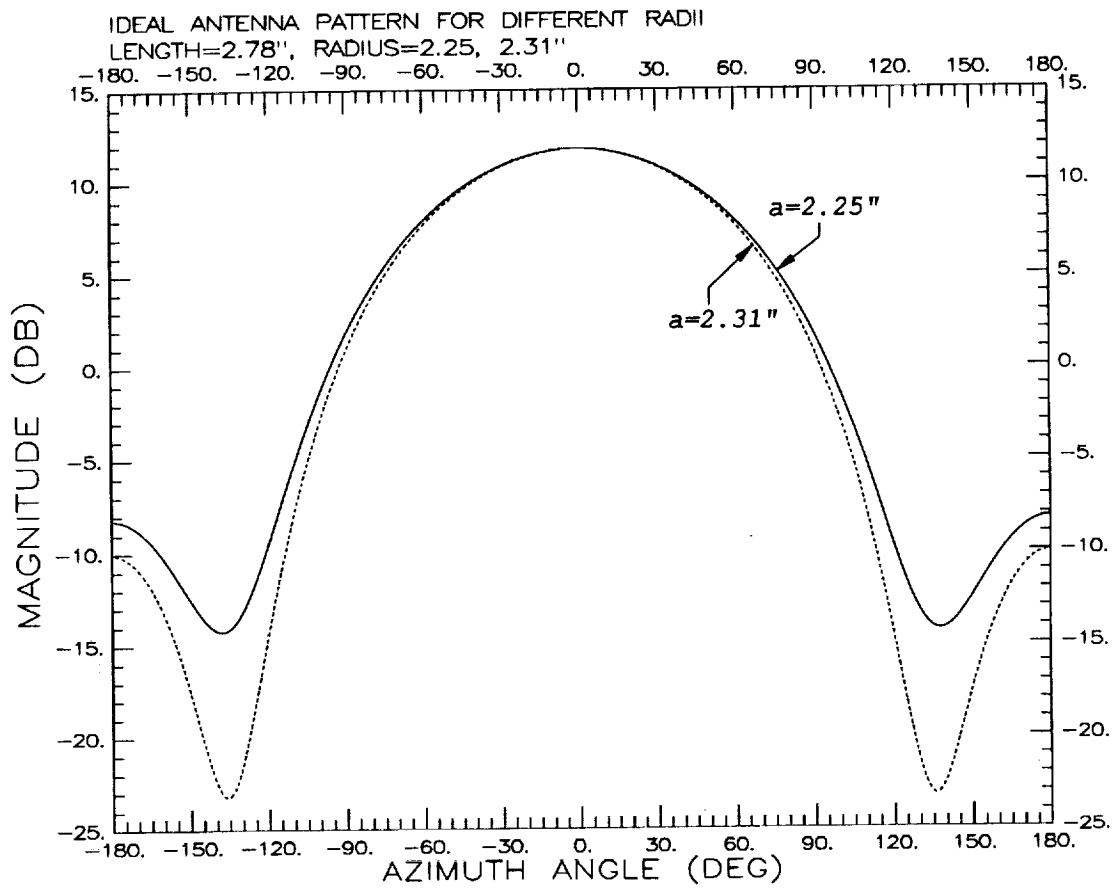


Figure 3.3: Antenna patterns for model where $a = 2.25''$, $2.31''$.

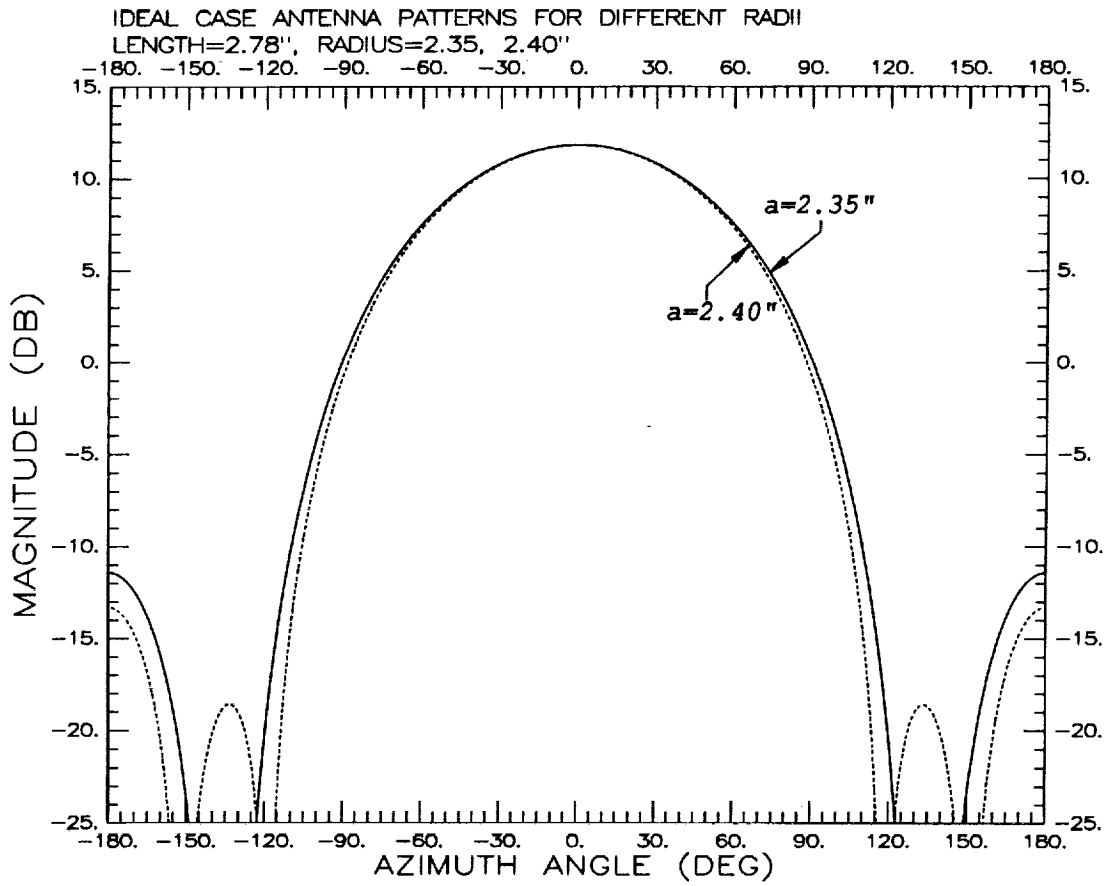


Figure 3.4: Antenna patterns for model where $a = 2.35'', 2.4''$.

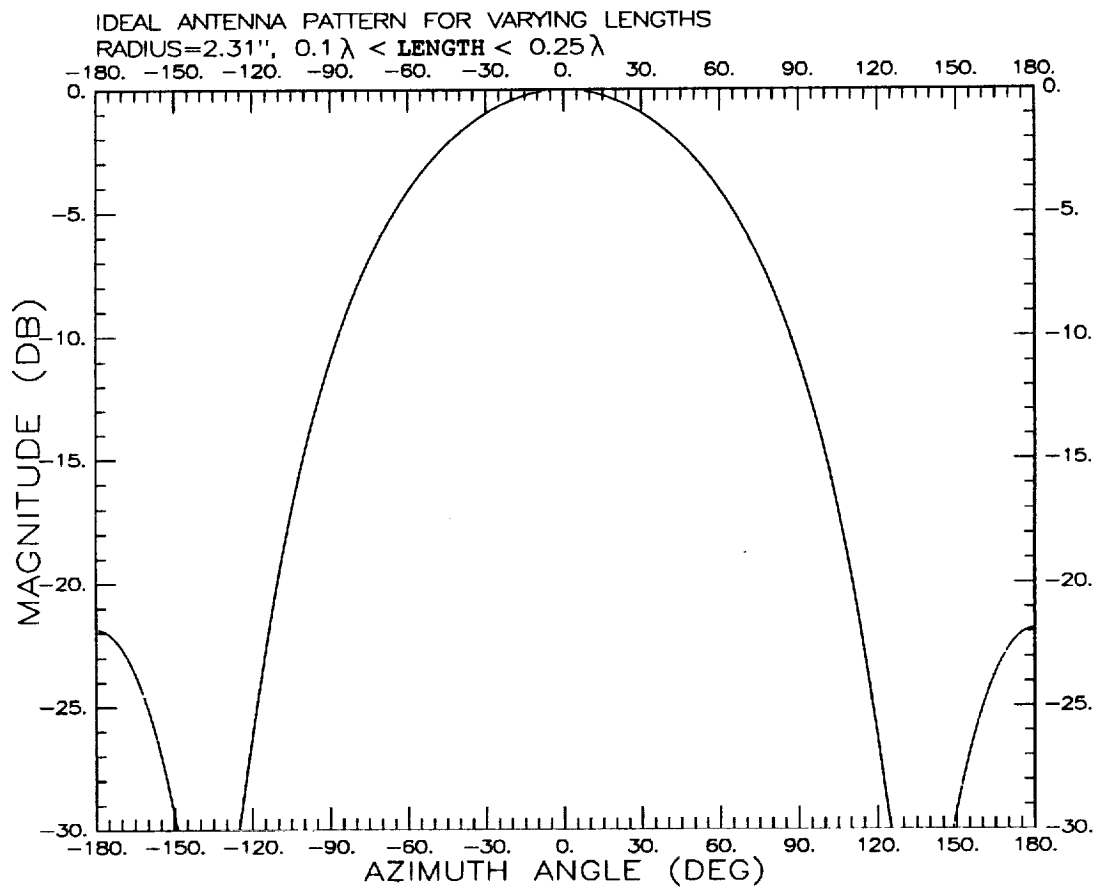


Figure 3.5: Normalized antenna azimuth patterns for length of element $l = \lambda/10, \lambda/6, \lambda/5, \lambda/4$ for radius of array $a = 2.31''$.

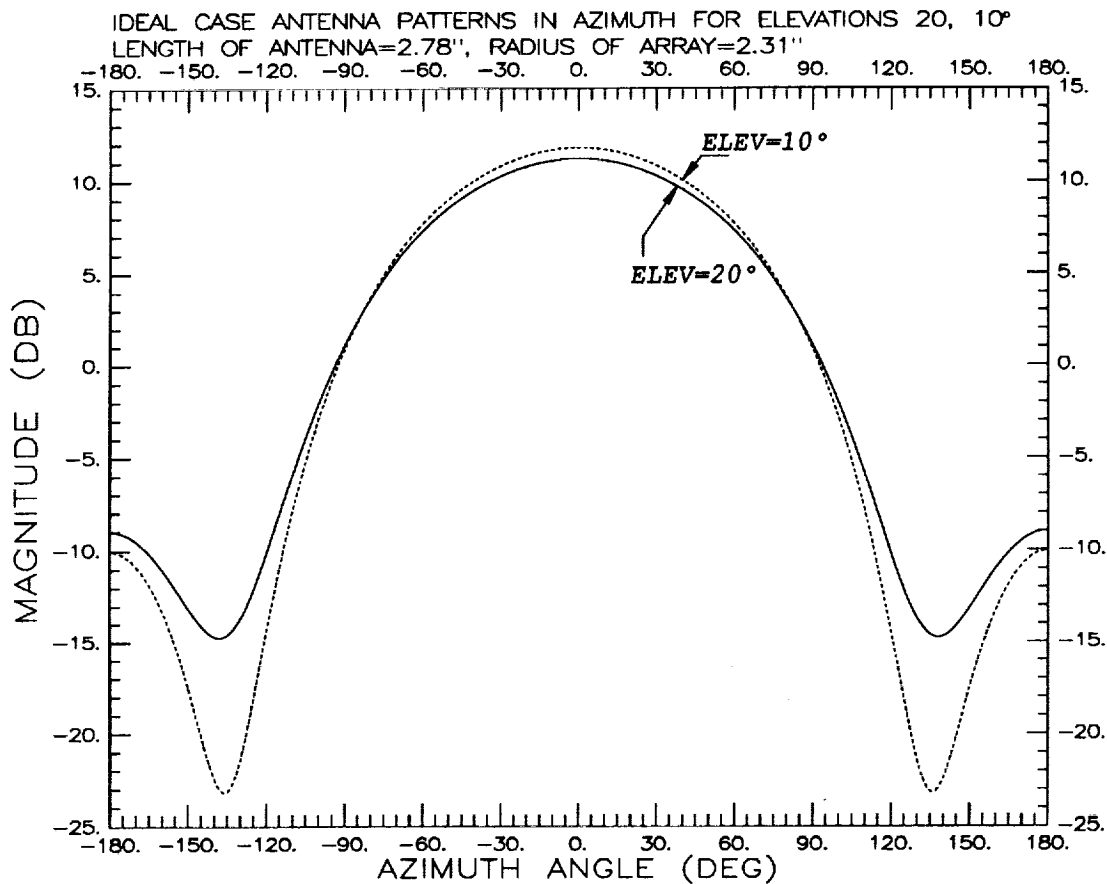


Figure 3.6: Variation of azimuth pattern at elevations 20, 10° for TCAS model with $a = 2.31''$, $l = 2.78''$.

From these results, the radius a and the length l that gives the best approximation to the specifications was picked for further computations with the aircraft code. Figures 3.6 and 3.7 show the pattern of the ideal TCAS model at various elevations.

The parameters of the ideal TCAS beam pointing at 0° are given in Table 3.2. It is found that the beam maxima in the four directions are no longer identical to each other due to the curvature of the fuselage. In

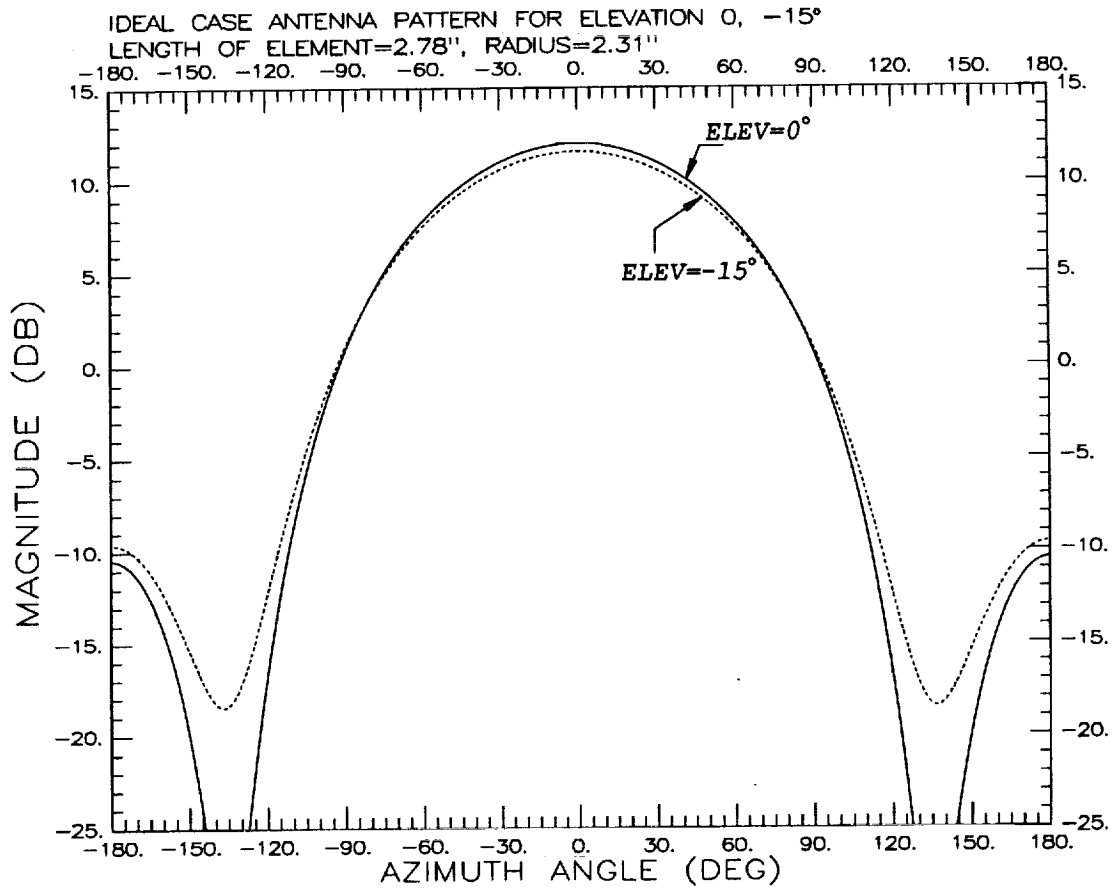


Figure 3.7: Variation of azimuth pattern at elevations 0, -15° for TCAS model with $a = 2.31''$, $l = 2.78''$.

Antenna radius (in)	ka (radians)	Beamwidth (°)		db drop at $\phi = 90^\circ$
		3 db	10 db	
Standard	—	90	180	10.00
2.25	1.27	105.0	180.0	10.0
2.31	1.30	102.0	174.0	10.9
2.35	1.33	101.0	170.0	11.6
2.40	1.35	99.0	167.0	12.6

Table 3.1: Variation of radiation pattern of TCAS antenna model on a ground plane with increasing radius ($f = 1060$ MHz).

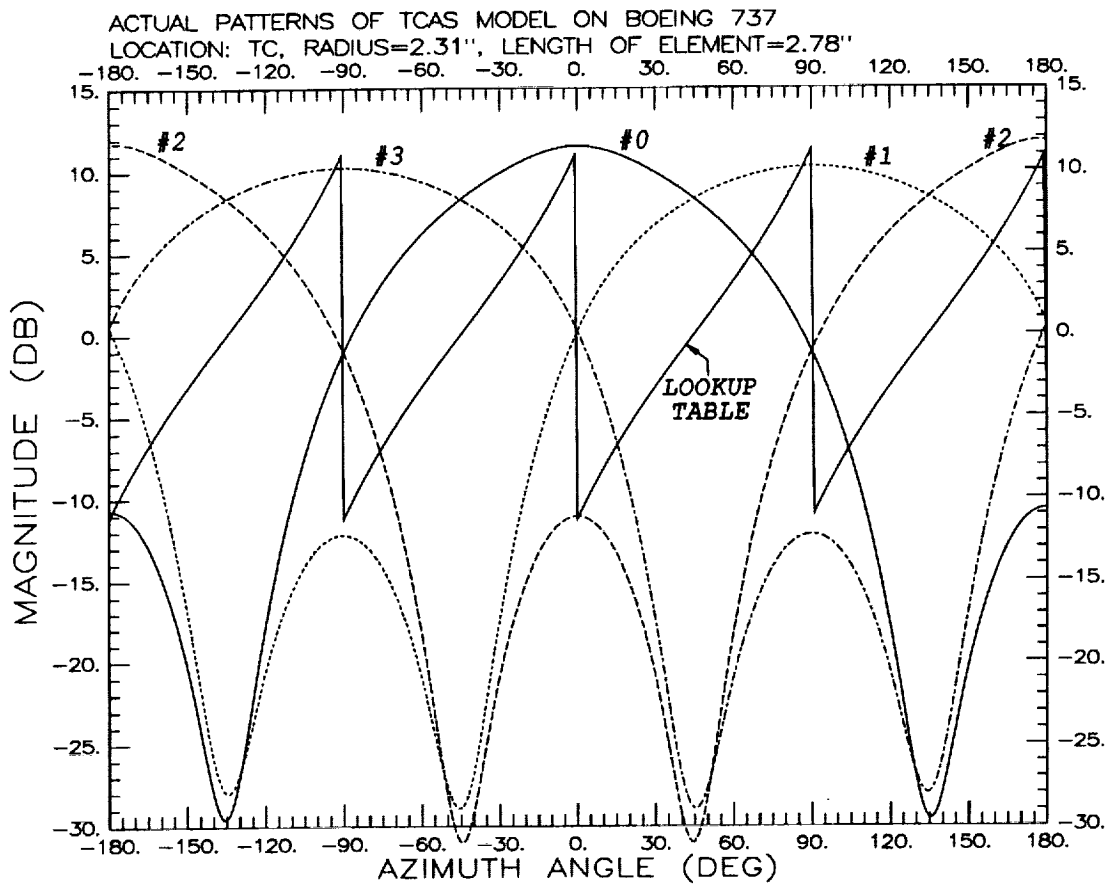


Figure 3.8: Actual patterns of TCAS model on Boeing 737-200 fuselage at location TC.

Figure 3.8, the four beams are shown for location TC (see also Table 3.5), about 378" from the nose, for an elevation of 10°. This was generated by the TCAS model on the Boeing 737-200 fuselage without any wings etc.

From this, a choice was made for the radius of the circular array. Note that $a = 2.25''$ was not chosen because the beam was too broad. Initially, $a = 2.35''$ was selected and tested on the fuselage model using the aircraft code. The beam was found to split up in the backlobe region into many

Location code	Distance from nose (")	Beamwidth ($^{\circ}$)		db fall at $\phi = 90^{\circ}$
		3 db	10 db	
Standard	378.6	90	180	10.00
TA	618.6	83.0	163.0	12.5
TC	378.6	86.0	163.0	12.5
TE	138.6	93.0	163.0	13.1

Table 3.2: Parameters of beam pointing at 0° at various locations on Boeing 737-200 fuselage for $a = 2.31''$ and $l_{monopole} = 2.78''$.

smaller lobes and an $a = 2.31''$ gave better results on this airplane model. This model also gave the best results for various locations of TCAS on the aircraft. After careful consideration of actual requirements, $a = 2.31''$ was chosen for this study. This was further supported by the supplied measured pattern for a TCAS antenna [12].

3.3 Simulation Algorithm for TCAS

The 4 element TCAS operates by a simple beam switching scheme. As mentioned in Chapter 1, the TCAS equipped aircraft transmits a beam at $f = 1030$ MHz in any of four preassigned directions, namely, 0° , 90° , 180° and 270° . Other similarly equipped aircraft (called 'intruder' from here on) responds with a coded reply while the enquiring aircraft listens omnidirectionally at $f = 1090$ MHz. In other words, the four beams are turned on in 'receive' mode. The dB values of the received signal are then compared and the two largest selected. Note that one also knows which receiver generated these signals. An estimate of the bearing of the intruder

is obtained by taking the difference of the dB values of the two largest received signals and comparing this value against a calibration or lookup table. Hereon, the difference of the two highest received signals will be referred to as the difference signal.

The TCAS is mounted on the fuselage without any other structural components and the four received signals at various bearings are computed. The azimuthal space is divided into four convenient quadrants namely, 0° – 89° , 90° – 179° , 180° – 269° , and 270° – 359° . Under ideal circumstances, the two channel numbers of the highest beams in each quadrant are known and one of these is selected as the reference signal. The other signal is subtracted from this reference signal to obtain a 'lookup table'. Since there are four beam directions, there are four monotonically increasing sections of the lookup table as shown in Figure 3.9. This table also stores the channel numbers of the two beams that generated any particular value of the lookup table. The table that lists the channel numbers and the reference signal for all possible ϕ is given in Table 3.3

Next, the various scatterers like wings, stabilizers etc., are added to the fuselage which leads to variations in the amplitude of the signals being received. Again, the difference signal is computed and stored along with the channel numbers in the 'wing table'.

To calculate the error, one starts with a given difference signal, the corresponding set of two highest received signals and their respective channel numbers for the case when the aircraft is simulated with wings, etc. From the channel number of the reference beam, one can place the intruder in

ϕ (degrees)	Highest Channel	Next Channel	Reference Beam
0-44	0	1	1
45-89	1	0	
90-134	1	2	2
135-179	2	1	
180-224	2	3	3
225-269	3	2	
270-314	3	0	0
315-359	0	3	

Table 3.3: Reference beams for the TCAS under ideal conditions.

Reference Beam #	Section of Lookup Table to search
1	0-89
2	90-179
3	180-269
0	270-359

Table 3.4: Location of intruder from received signals under ideal conditions.

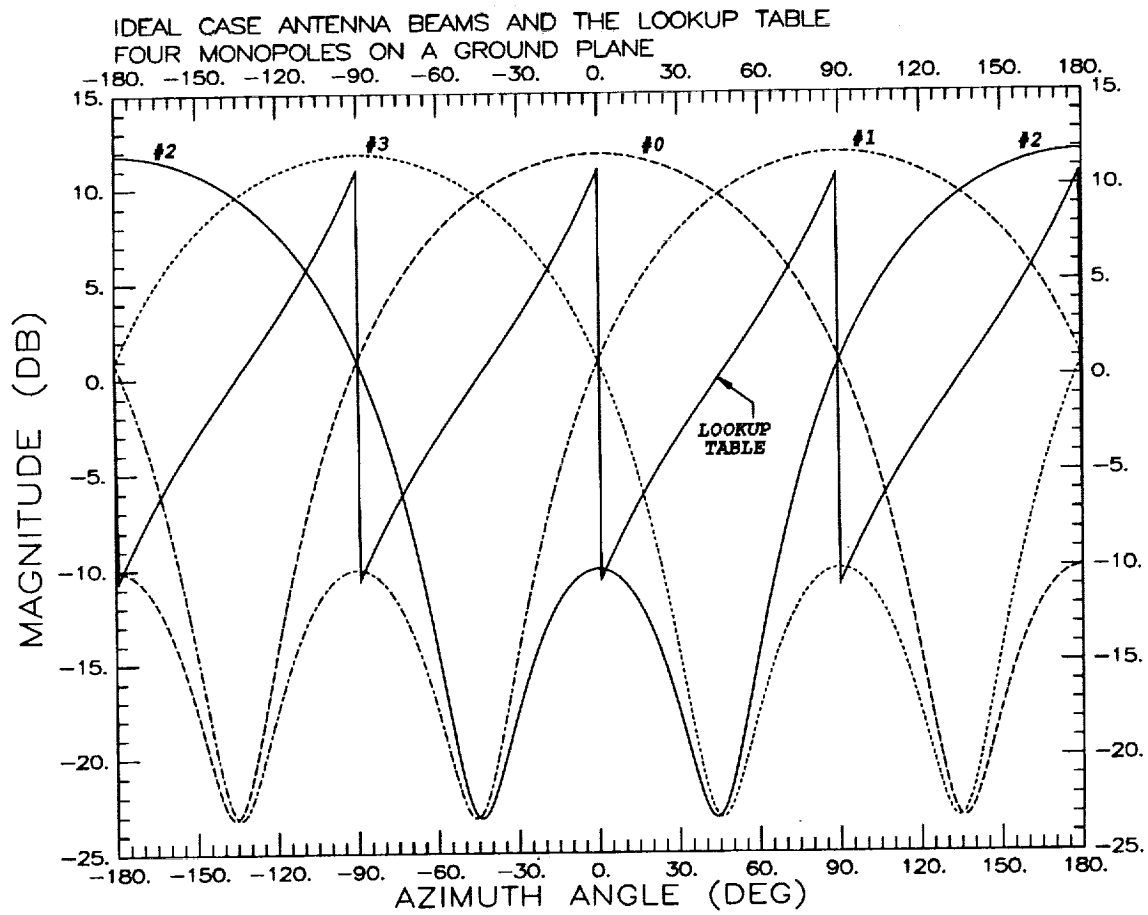


Figure 3.9: Creation of receiver beams and the lookup curve.

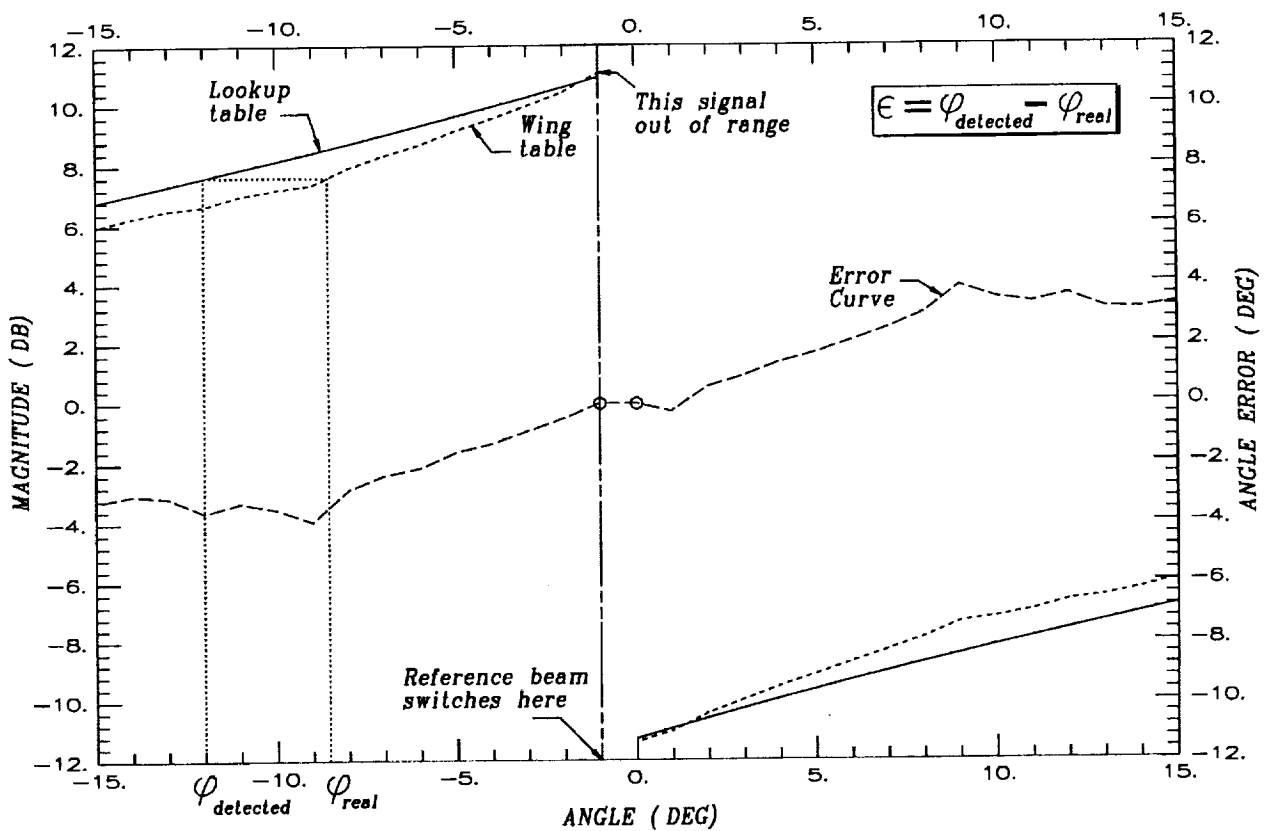


Figure 3.10: Calculation of bearing error.

one of the four quadrants. This is shown in Table 3.4. That section of the lookup table is then searched for the same value of difference signal as illustrated in Figure 3.10. A linear interpolation scheme is used to find the predicted bearing when the difference signal lies between two points on the lookup table. The error ϵ , is then calculated as

$$\epsilon = \phi_{\text{detected}} - \phi_{\text{real}}. \quad (3.6)$$

There are two sources of ambiguity/uncertainty that arise here. If the difference signal lies outside the range of the lookup table; i.e., the two

highest received signals are a valid combination of beams but the value of the difference signal is not within the boundaries of the lookup table. Then, an 'out of range' warning is generated as shown in Figure 3.10 and the error is set to the extreme value of the lookup curve. Another source of error occurs when two beams that have opposite bearings are received as the highest signals because of scattering. This leads to an illegal combination of channels and one cannot calculate a table entry for this ϕ . This leaves the processor with no lookup table to search. Hence, the bearing of the intruder cannot be estimated. The error is set equal to the previous value of error and a 'no lookup table' warning is given and the plot is marked accordingly.

3.4 Results and Discussion

In this section, results are provided for the case of a top mounted TCAS (on a Boeing 737-200) antenna based on the algorithms described in Sections 3.2-3.3. The engines were not included in the model because they are far from the antenna and are shadowed by the fuselage. These results show the error in estimating the bearing of the intruder when the TCAS is mounted on top of a Boeing 737-200 at three locations. The headers in these plots also contain some useful information for quick reference. The first line of the header gives the number of elements in the antenna system, the location of TCAS (i.e., top or bottom mounted), and the elevation angle, respectively. The second line gives the statistical information about the forward quadrant, ie, $-45^\circ \leq \phi \leq +45^\circ$ range. Absolute value of maximum

Antenna Location	Z coordinate (inches)	Distance from nose (inches)
TA	310.0	618.6
TC	70.0	378.6
TE	-170.0	138.6

Table 3.5: Locations of TCAS on top of Boeing 737-200.

detected bearing error in this range, average and standard deviation of the bearing error are also given. This quadrant is also referred to as the 'nose' quadrant. The third line gives information about the location of the antenna, distance from the nose and any other relevant information about the model. Notice that the plots are all antisymmetric about 0° . This is because the antenna is mounted on top of the fuselage at its centerline, and the aircraft is a symmetric body. The oddness of symmetry is because the way the error is computed, as explained earlier.

The plots are also marked where the previously discussed error conditions occur. The locations of TCAS used here, labelled TA, TC, and TE (where the first character T denotes a top mounted antenna) correspond to A, C, and E in [6], respectively. The details about these locations are tabulated in Table 3.5 and views of the model are given in Figure 3.11. Error curves are given for four elevations: $+20^\circ$, $+10^\circ$, 0° , and -10° . The statistics about maximum error, etc., for the antenna at these locations are given in Appendix A. Note that the parameters given in the appendix, i.e., maximum, average and the standard deviation of the bearing error are for absolute values of the error.

One notices a surprising similarity in some of the error curves between the 8 element monopulse system and the 4 element amplitude system. This is partially due to the fact that the model of the aircraft used was the same for both locations, even though the antennas and the method of operation are completely different. One can also see the jumps in some of the error curves for the four element amplitude system which are not present in the eight element monopulse system error curves. This seems to be an inherent problem in the operation of the amplitude system. Figure 3.12 shows a part of the error curve around a point where there is such a jump. This data corresponds to location TC, at 20° elevation, around the 80°–100° region. It is seen in this instance that, the wing table values are always lower than the lookup table values. Consider two cases:

Case 1: $\phi_{real} \leq 90^\circ$.

Say, the difference between the two highest received signals has a magnitude of 10.08 dB (for actual bearing of intruder $\phi_{real} = 90^\circ$) and the two highest channels are 0 and 1. This tells that the intruder lies in the 0–90° quadrant. Searching the corresponding section of lookup table, one finds that $\phi_{detected} \approx 86.5^\circ$. The error is then, $\epsilon_1 = \phi_{detected} - \phi_{real} \approx -3.5^\circ$.

Case 2: $\phi_{real} > 90^\circ$.

Consider again the case when magnitude of difference between two highest channels is about -10.03 dB (for actual bearing of $\phi_{real} = 91^\circ$) and the highest channels are 1 and 2. Then, searching the relevant section of the lookup table, the detected position of intruder is determined as $\phi_{detected} \approx 93.8^\circ$ to give an error of $\epsilon_2 = \phi_{detected} - \phi_{real} \approx +2.8^\circ$.

Now, it can be seen that the jump in the error curves is occurring be-

cause of beam switching and due to the slight change of the beams as a function of elevation which are depicted in Figures 3.6 and 3.7. This can be seen more clearly in top picture of Figure 3.13 where two calibration curves calculated at 10° and 20° are shown. If one calculates an error curve where the calibration curve at 10° is used as a reference and the calibration curve at 20° as the received signal, the result is an error curve which is discontinuous at -90° , 0° , 90° , and 180° as illustrated in bottom picture of Figure 3.13. A similar calculation also shows that there is no discontinuity in some of the error curves, especially those close to the elevation for which the lookup table was created. This is probably the most serious drawback of the four element system.

At location TA, which is 618.6 inches from the nose, the error curves for the 4 element TCAS meets the specifications only in the nose quadrant; however, its performance in this quadrant is slightly better than the 8 element TCAS mounted at the same location. As expected, the performance of the 4 element amplitude comparison system is not as good as the 8 element monopulse system in the left and right quadrants. This result is due to the fact that the 4 element TCAS antenna transmits beams in the directions 90° and 270° where they are distorted by the wings. The 8 element monopulse system also transmits a sum beam in these directions, however, unlike the 4 element TCAS it also transmits a difference beam. Note that both systems do not perform very well in the tail quadrant due to the presence of vertical stabilizers. At an elevation of $+10^\circ$ the statistics show that the TCAS III performs much better in the left and right quadrants (collectively called the 'side' quadrants from here on). The maximum

error of 8 element TCAS III is well within the 2° limit and the 4 element TCAS just so. The maximum error exceeds the 2° limit at many azimuth angles. In the tail region, both antennas do not meet the specifications.

At 0° elevation, the 4 element amplitude system is slightly better than the 8 element monopulse system in the nose quadrant. However, the 8 element TCAS III performs better in the side quadrants. The statistics of error for the tail region are similar. As expected, the performance at -10° is unacceptable for both systems. There is a remarkable similarity in the shape of the two error curves; however the ripples in the error curve are usually more pronounced for the 4 element amplitude system. Notice that in both cases, the standard deviation is quite large compared to the magnitude of average error.

Next, at location TC, which is 378.6 inches from the nose one notices that the monopulse system of TCAS III is better than the 4 element amplitude system in all quadrants at 10° . Even though the average and standard deviation are within 2° , the maximum error exceeds this number in all quadrants except in the nose quadrant where both antennas meet the specifications. Again, one notices the jump in the error curve (for the 4 element array) for an elevation of 20° , which is not present in the 8 element system. It is also found that the maximum error is much higher for the four element TCAS. These observations also hold for elevation of 0° for both antennas. Again, the 4 element TCAS is somewhat better than TCAS III in the nose quadrant. One also notices the tendency of the error curve to be discontinuous at beam switching points. The errors in the tail quadrant are too great for either system to be of much use. The 4 element

TCAS also exhibits higher error in the side quadrants. It is interesting to see that the performance is worse in the side quadrants at -10° than the tail quadrants due to scattering from wings.

Finally, at TE, which is closest to the nose at 138.6 inches, the 4 element TCAS does not meet the requirements at 20° elevation. The error curve is also discontinuous at all beam switching angles. The error curve for the 8 element monopulse system is smooth and the performance of the system is more acceptable. At 10° however, both antennas perform well in the nose quadrant. Further, TCAS III meets these specs in the side quadrants also as opposed to the 4 element TCAS.

Unlike the previous locations, at 0° elevation, TCAS III is better than the 4 element version in the nose quadrant where its performance is acceptable. This is not the case for 4 element TCAS whose performance at this location is the worst among those considered in this report. The error parameters of both antennas in other quadrants also indicate that the 8 element TCAS III is a better system.

A comparison of various statistical parameters of the error curves for the four and eight element TCAS at elevations 10° and 0° at location TC are given below. This is a subset of data in Appendix A. The data for nose and tail quadrants is summarized in Tables 3.6 and 3.8 respectively. The statistical parameters for 20° and -10° elevations at location TC are also presented in Tables 3.9-3.11. It is interesting to find that even though the magnitude of error is higher, the performance of both antennas is about the same in the tail quadrant. The error curve data for the left and right quadrants are averaged and given in Tables 3.7 and 3.10. In this case also,

Parameter of interest	Elevation=10°		Elevation=0°	
	4 element	8 element	4 element	8 element
Abs. Maximum	0.106	0.021	0.800	1.279
Abs. Average	0.033	0.001	0.397	0.914
Std. Deviation	0.023	0.004	0.234	0.317

Table 3.6: Comparison of TCAS error curves for location TC in the nose quadrant at 10° and 0° elevations.

Parameter of interest	Elevation=10°		Elevation=0°	
	4 element	8 element	4 element	8 element
Abs. Maximum	8.252	2.814	2.438	1.904
Abs. Average	0.652	0.467	1.068	0.600
Std. Deviation	0.992	0.571	0.469	0.369

Table 3.7: Comparison of TCAS error curves for location TC in the side quadrants at 10° and 0° elevations.

the eight element TCAS III performs slightly better than the four element TCAS.

The performance of the four element TCAS is generally not as good as the eight element TCAS III, except in the nose quadrant where it performs as well as the monopulse system, and sometimes slightly better. This is mainly due to the method used for direction finding. The four element TCAS operates on a beam switching technique which is more sensitive to the various structural scatterers of an airplane, i.e., wings, engines, tail, etc. The beam switching technique and the slight variation of the four beams as a function of elevation also gives rise to the 'jumps' referred to above. In order to minimize these jumps, it is necessary to choose an optimum

Parameter of interest	Elevation=10°		Elevation=0°	
	4 element	8 element	4 element	8 element
Abs. Maximum	3.684	3.562	5.200	5.662
Abs. Average	1.353	1.157	1.109	1.169
Std. Deviation	0.979	0.862	1.033	1.014

Table 3.8: Comparison of TCAS error curves for location TC in the tail quadrant at 10° and 0° elevations.

Parameter of interest	Elevation=20°		Elevation=-10°	
	4 element	8 element	4 element	8 element
Abs. Maximum	2.466	0.600	3.919	4.529
Abs. Average	1.042	0.280	2.586	3.401
Std. Deviation	0.743	0.160	0.806	1.050

Table 3.9: Comparison of TCAS error curves for location TC in the nose quadrant at 20° and -10° elevations.

Parameter of interest	Elevation=20°		Elevation=-10°	
	4 element	8 element	4 element	8 element
Abs. Maximum	3.667	2.527	30.16	8.483
Abs. Average	1.424	0.553	2.475	1.471
Std. Deviation	0.860	0.387	2.851	1.237

Table 3.10: Comparison of TCAS error curves for location TC in the side quadrants at 20° and -10° elevations.

Parameter of interest	Elevation=20°		Elevation=-10°	
	4 element	8 element	4 element	8 element
Abs. Maximum	16.30	6.482	6.425	6.579
Abs. Average	2.987	1.609	3.186	4.280
Std. Deviation	3.323	1.523	1.193	1.245

Table 3.11: Comparison of TCAS error curves for location TC in the tail quadrant at 20° and -10° elevations.

length of the monopulse radiator such that the radiation pattern does not change much as a function of elevation within the range -15° to +20°. The bearing of an intruder is found from the difference of two beams which are both slowly varying with ϕ . On the other hand, the TCAS III operates on a monopulse principle which utilizes both a maximum and a null in the approximate direction of the intruder to locate it more accurately. The discontinuities seen in the four element system error curve are also absent. It seems that in directions where there are no scatterers, both systems perform well; however, in directions where there are scatterers; i.e., right, left and tail quadrants, the monopulse system performs better.

The performance of the 4 element TCAS is acceptable ($|\epsilon| \leq 2^\circ$) in the forward direction for the locations TA and TC within the elevation range 0°-10°. It is found that in case of location TE, the one closest to the nose, the error is too great even for 0° elevation. One also notices that the error is minimum for elevation of 10° because that is the angle at which the lookup table was created. Thus, as the elevation gets higher or lower, the error tends to increase.

Another observation is that the tables for the 4-element amplitude sys-

tem tend to get "out of range" more often when the elevation angle is small or negative. The errors due to the processor detecting a target but not being able to locate its bearing in a lookup table due to an invalid combination of the largest two beams is more serious. This usually occurs for low elevation intruders mostly in the tail region. This can be attributed to the effect of the tail which distorts the transmitted beam. That is why the error is oscillatory and large in the tail quadrant.

In summary, it is evident that both antennas are similar in performance in the nose quadrant and usually meet the specs in the vicinity of 10° elevation. In all cases considered, the 8 element TCAS III is better than the 4 element TCAS in the left and right quadrants. Both antennas are comparable in the tail region though both antennas do not meet the guidelines for acceptable performance. An advantage of the 4 element amplitude system is that it is simpler than the monopulse system and therefore less expensive to build.

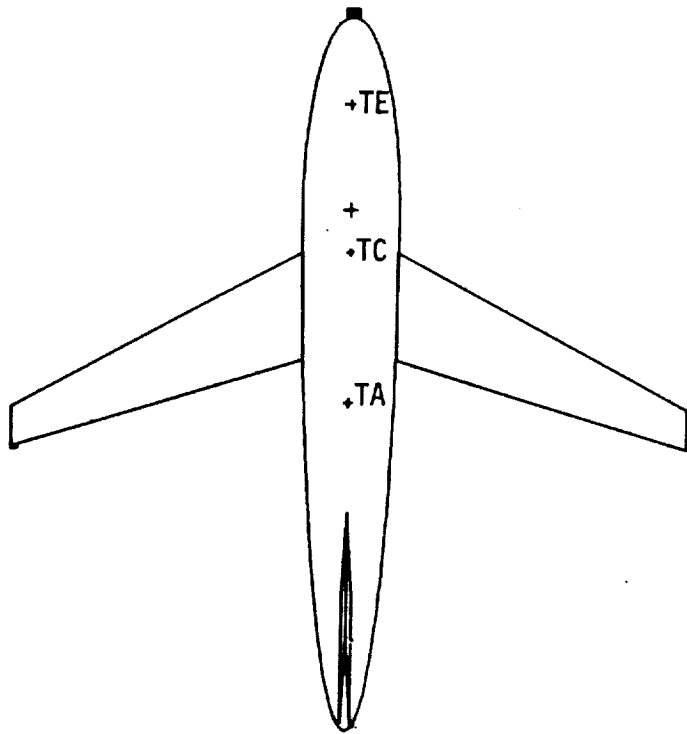
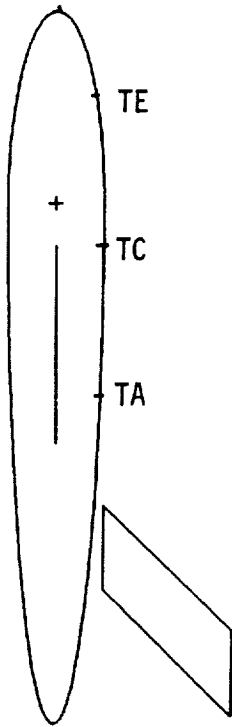
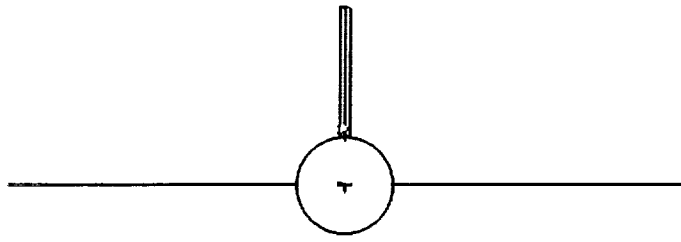
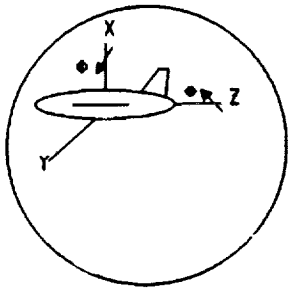


Figure 3.11: Model of Boeing 737-200 for a top mounted TCAS antenna.

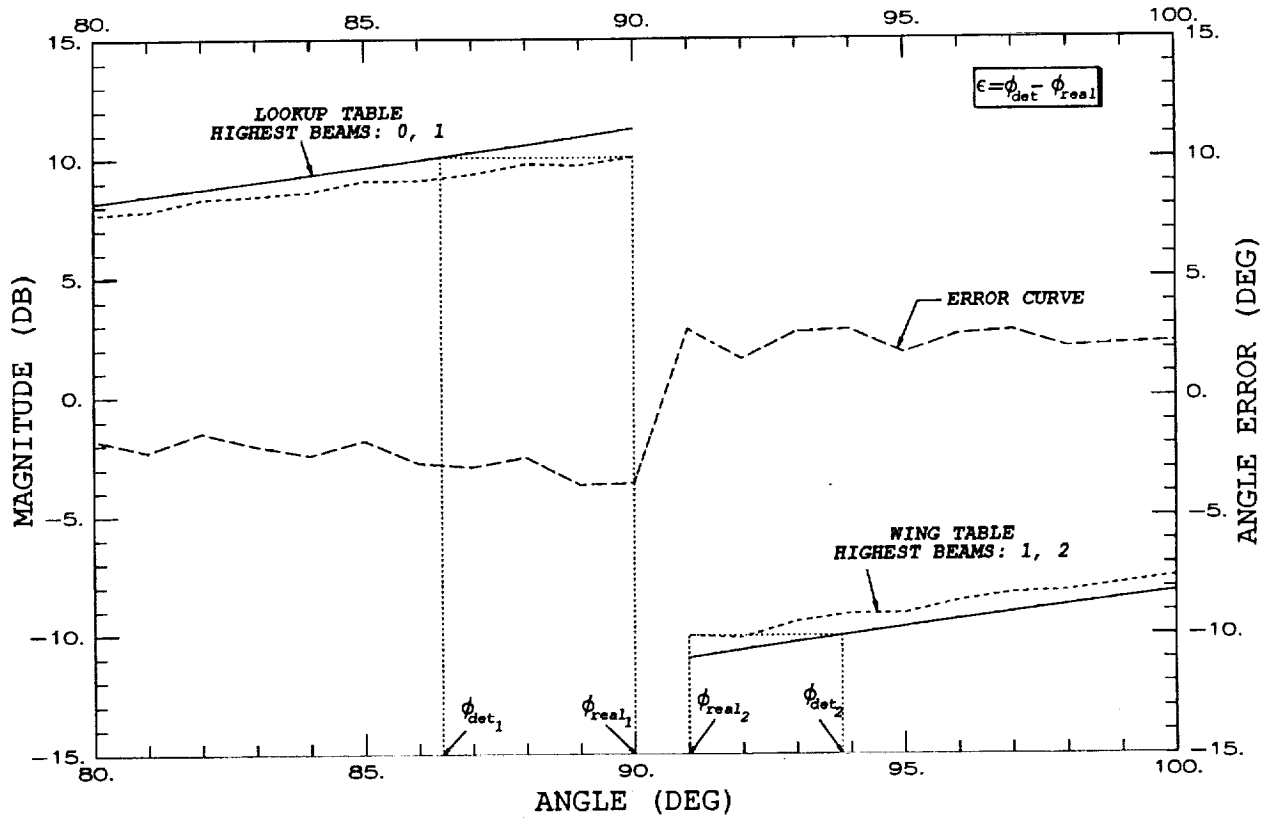


Figure 3.12: Explanation for discontinuities in the error curve. Data corresponds to location TC about 378" from nose, at 20° elevation.

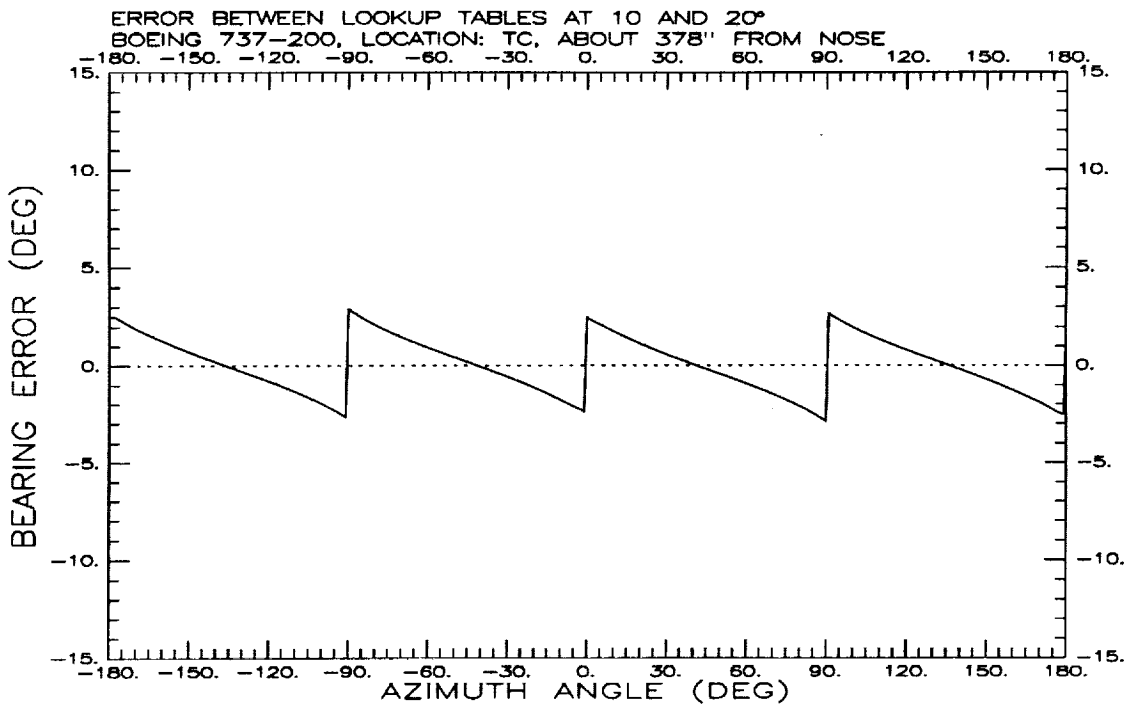
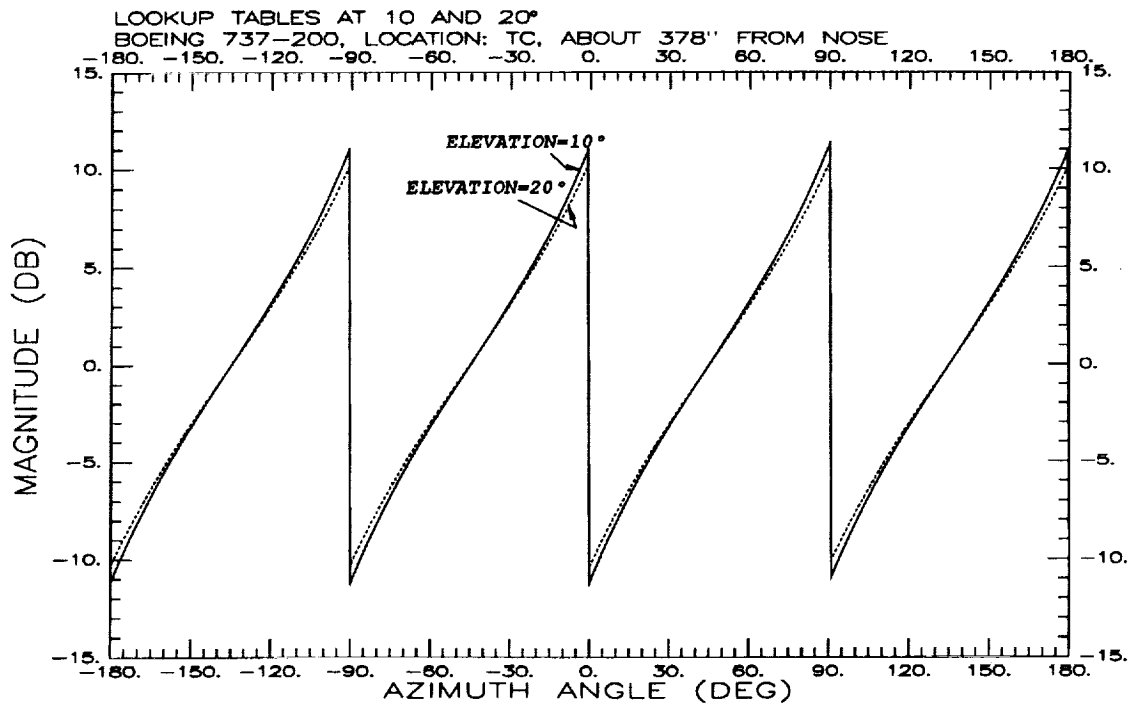


Figure 3.13: Explanation for jumps in the error curve for 4 element TCAS. Data corresponds to location TC.

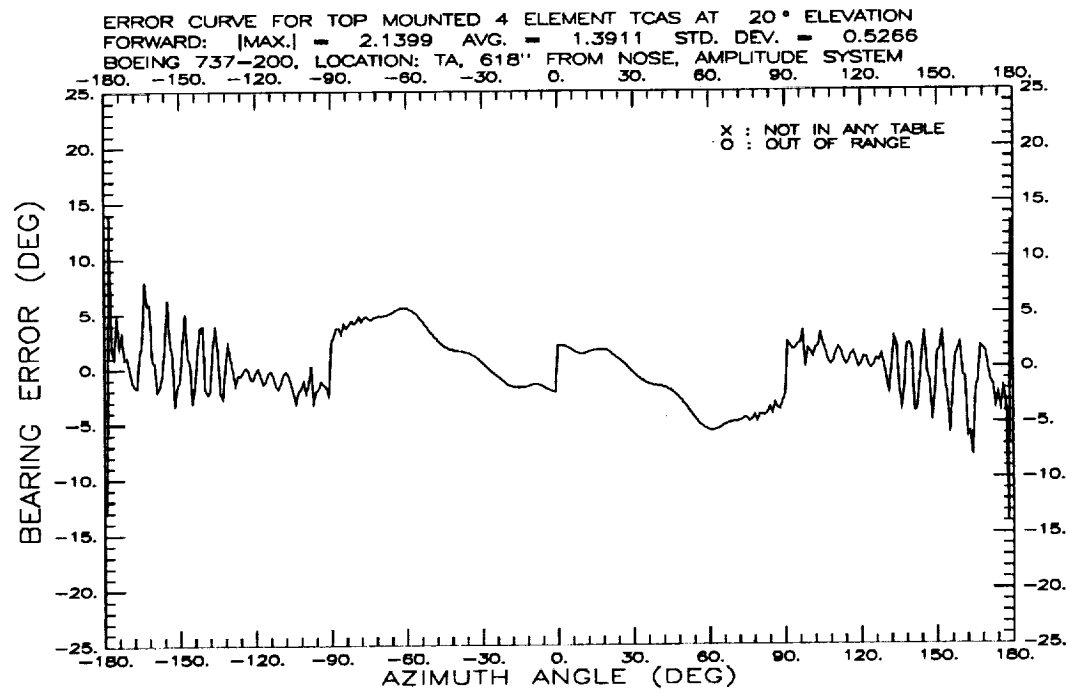
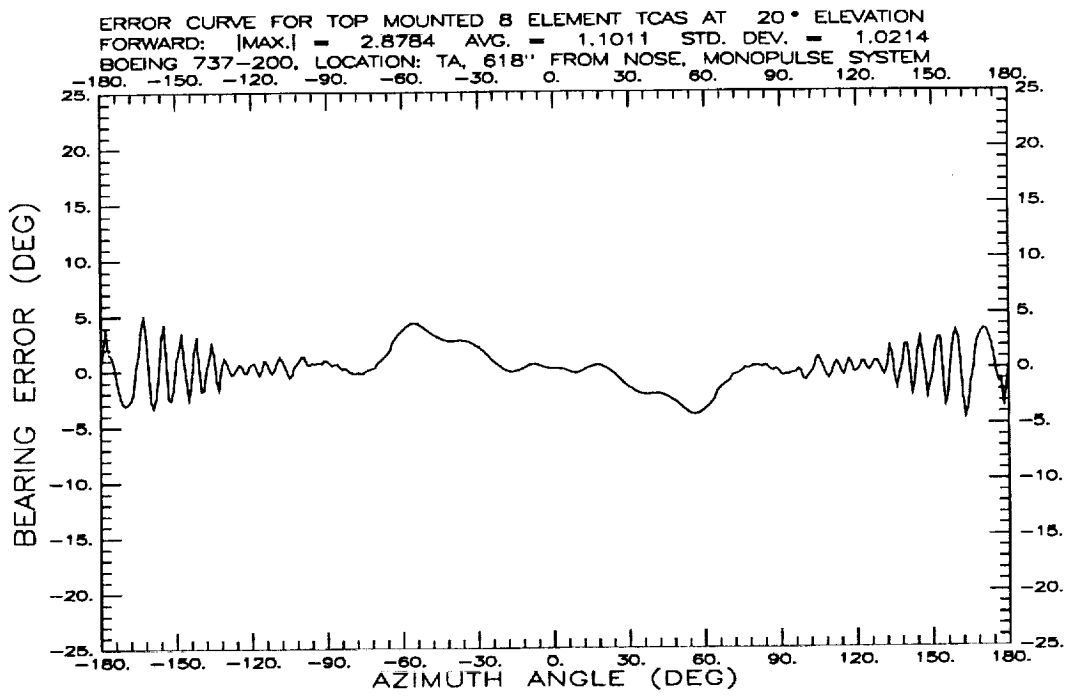


Figure 3.14: Error curve for 8 (top) and 4 (bottom) element TCAS at TA about 618.6" from nose at +20°.

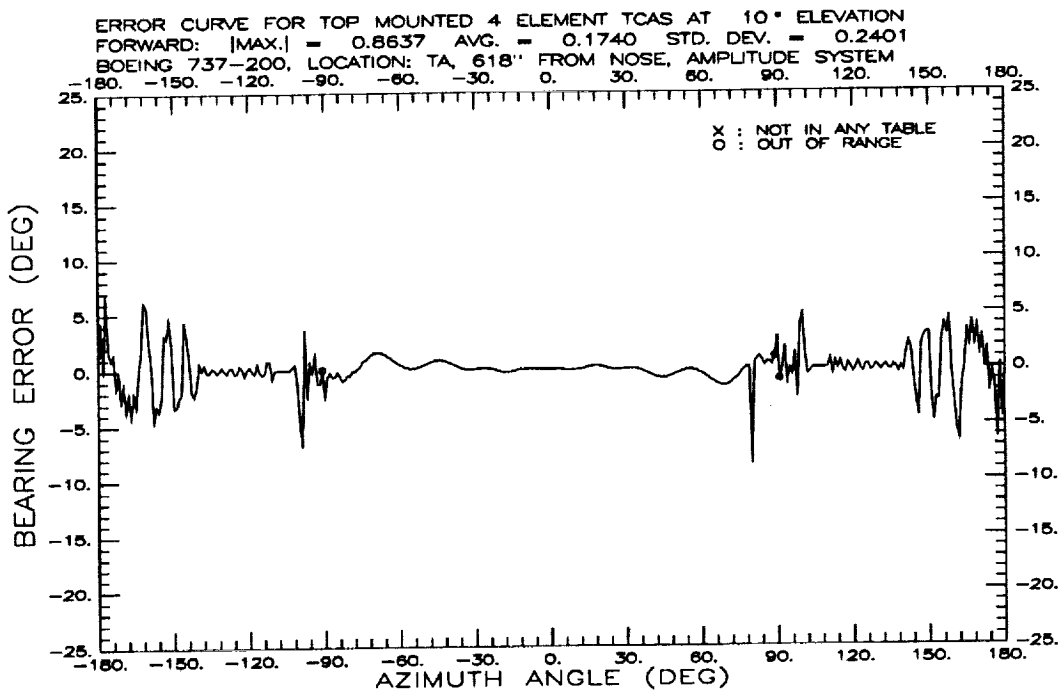
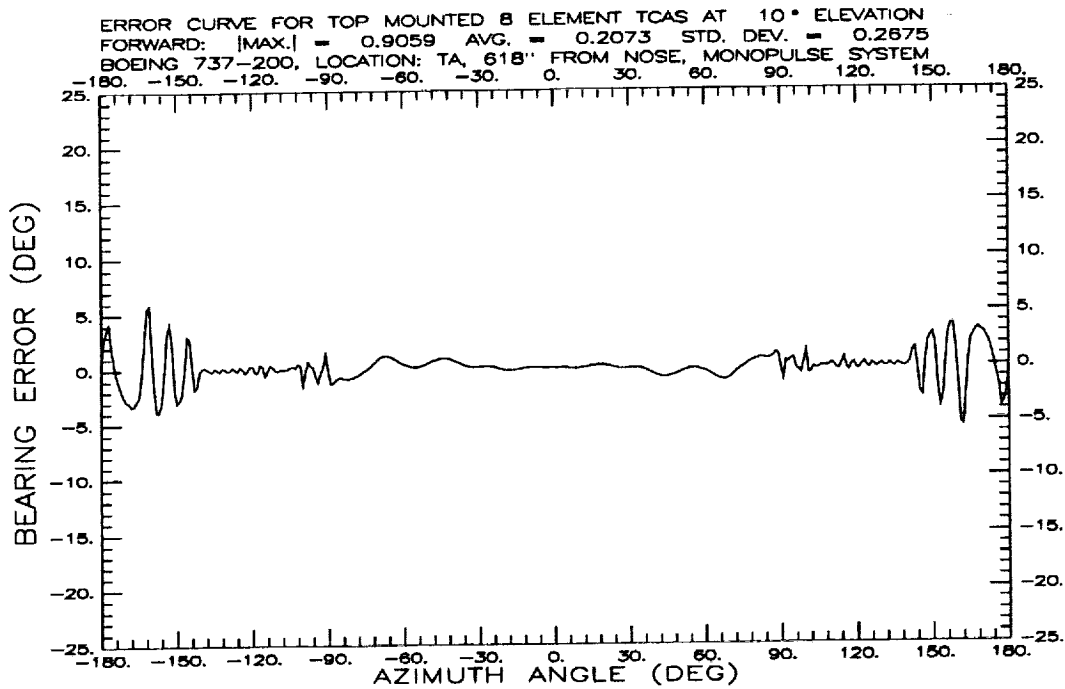


Figure 3.15: Error curve for 8 (top) and 4 (bottom) element TCAS at TA about 618.6" from nose at +10°.

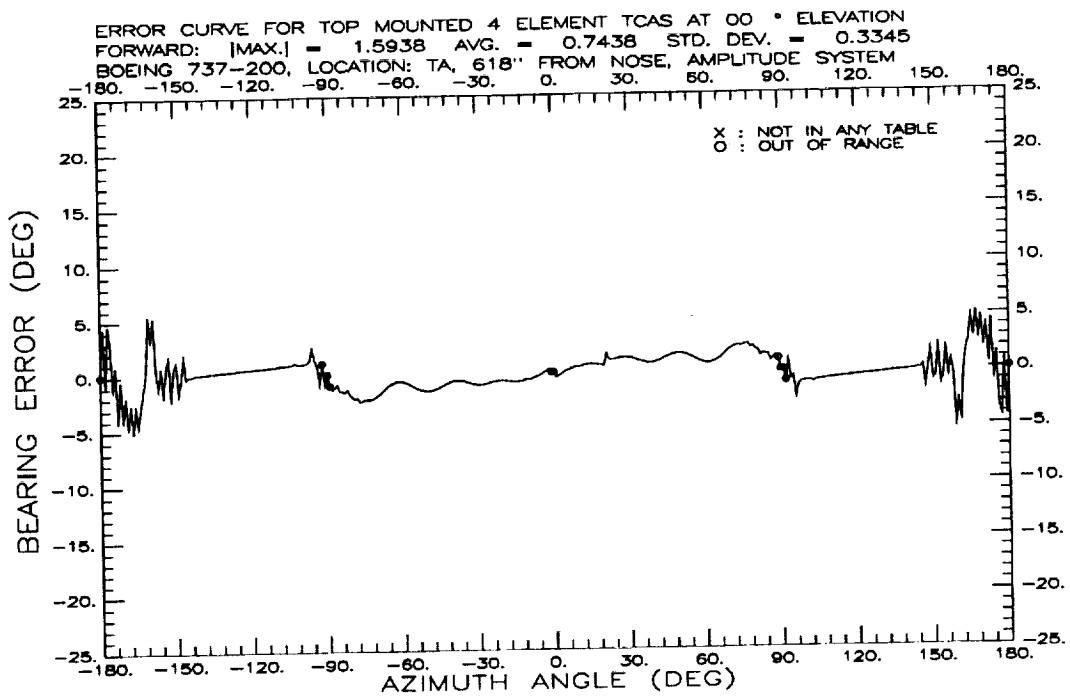
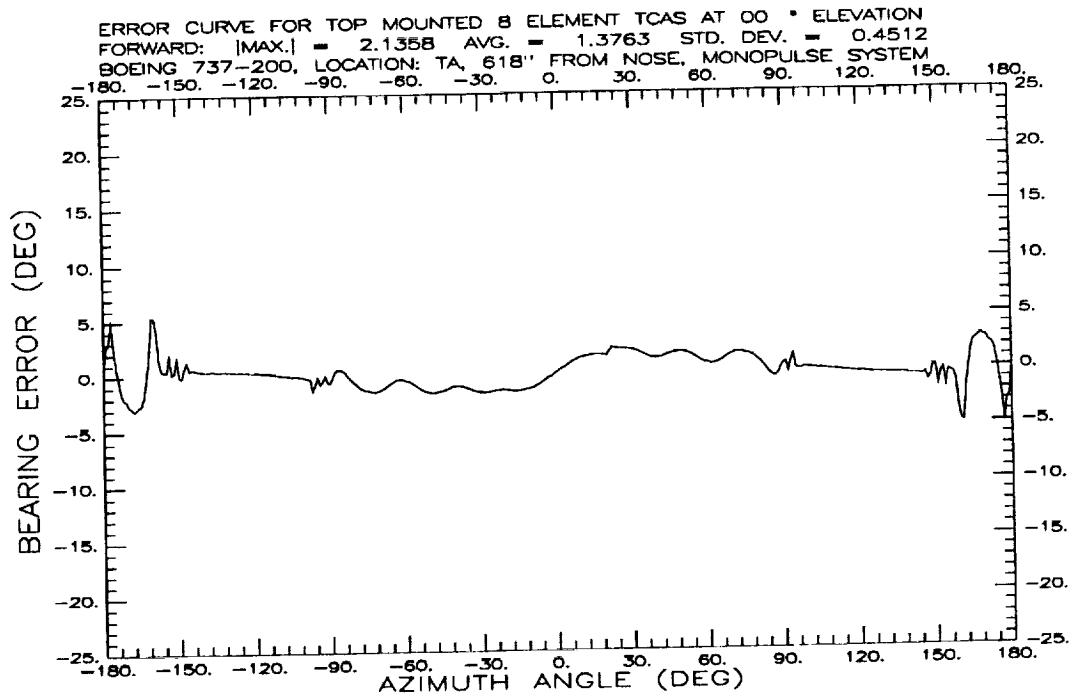


Figure 3.16: Error curve for 8 (top) and 4 (bottom) element TCAS at TA about 618.6" from nose at 0°.

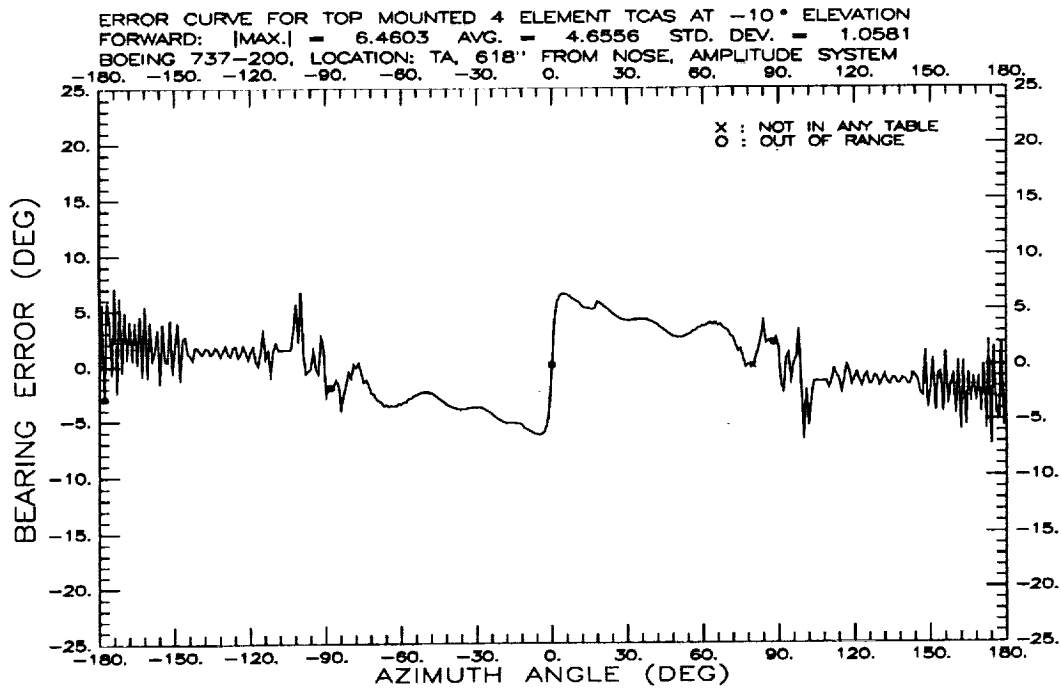
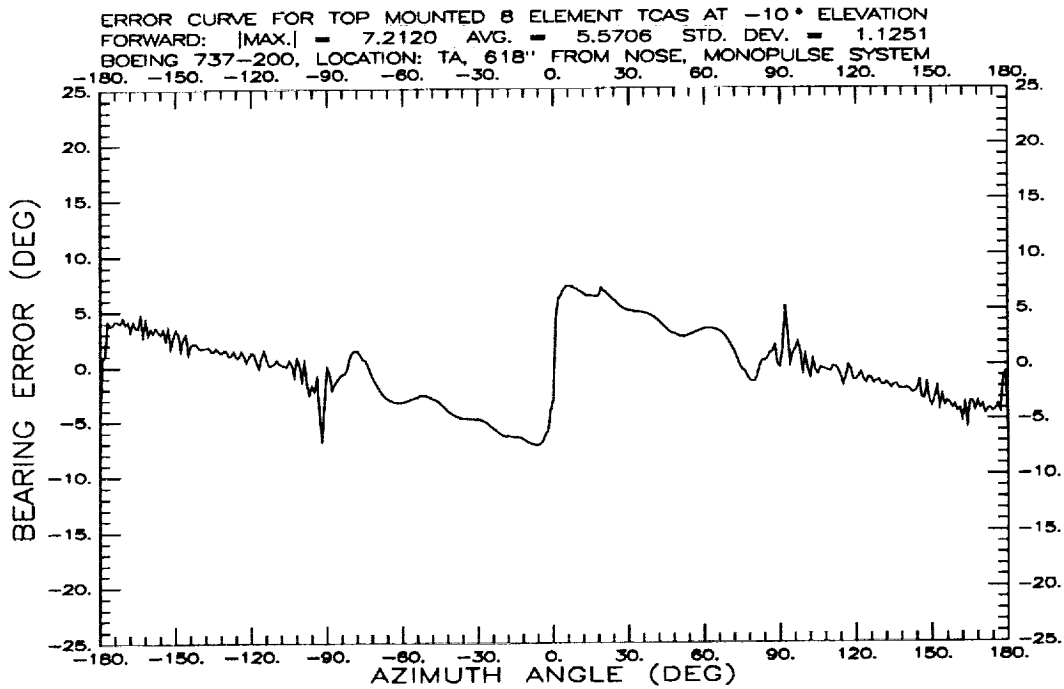


Figure 3.17: Error curve for 8 (top) and 4 (bottom) element TCAS at TA about 618.6" from nose at -10° .

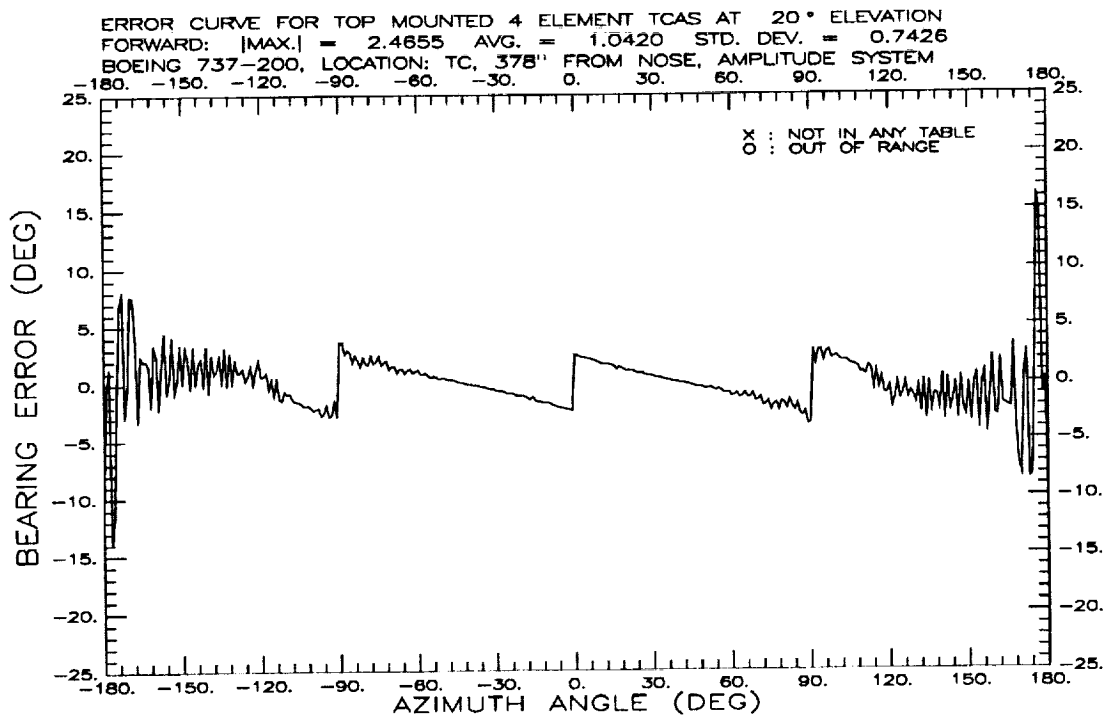
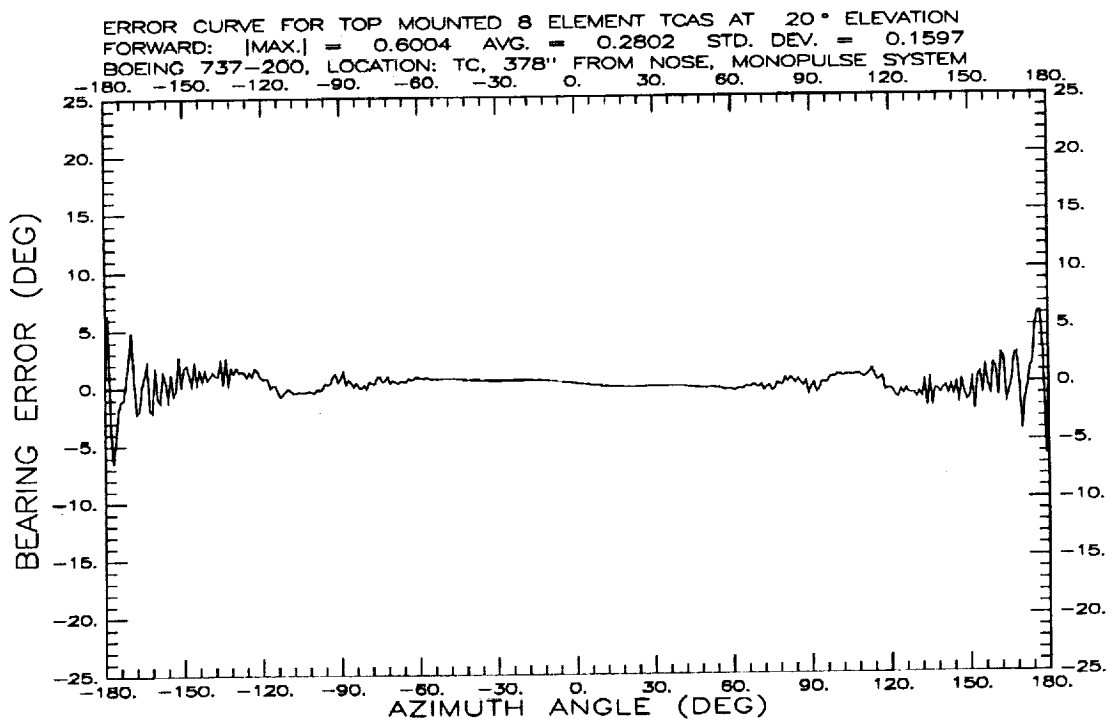


Figure 3.18: Error curve for 8 (top) and 4 (bottom) element TCAS at TC about 378.6" from nose at +20°.

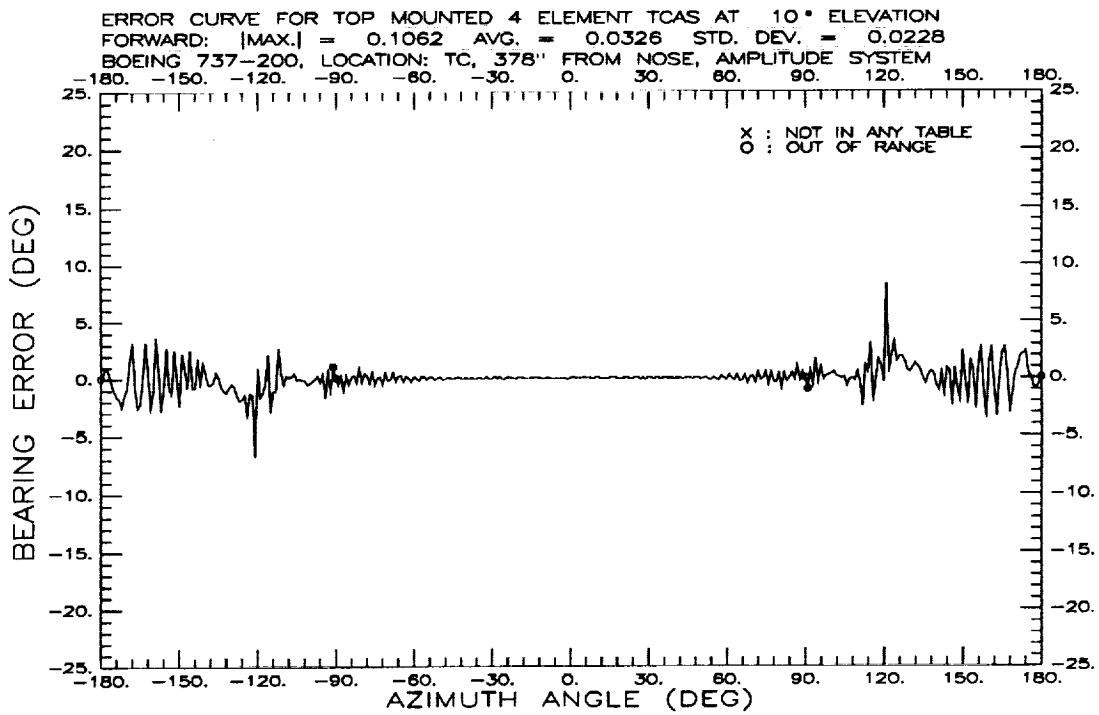
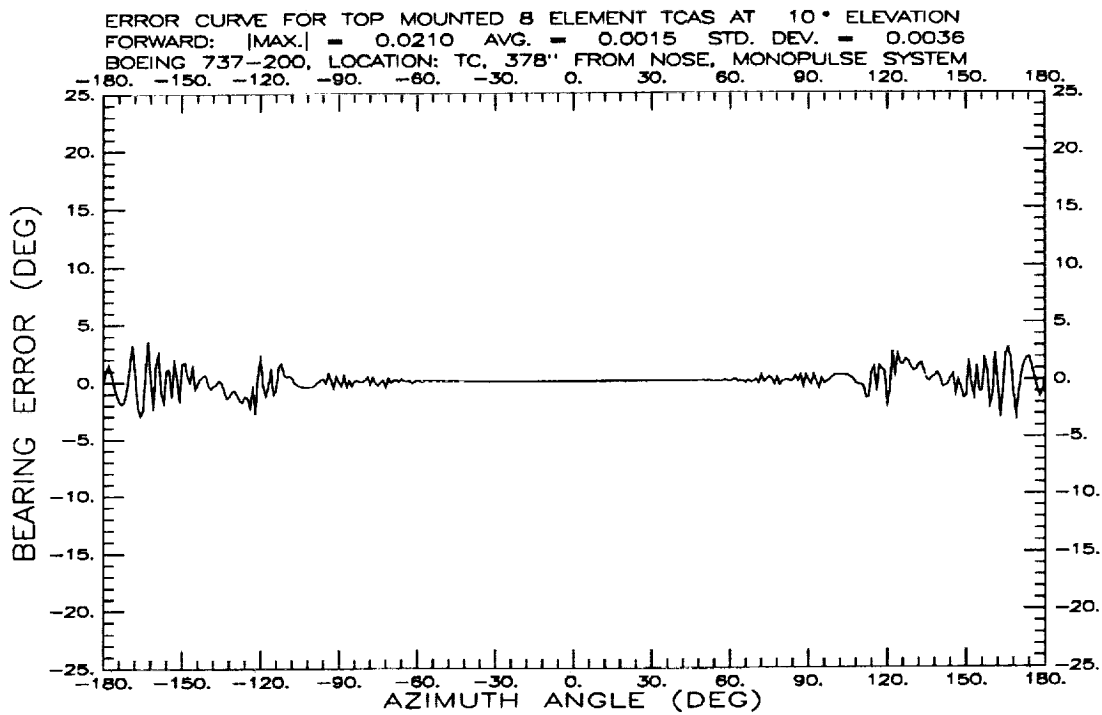


Figure 3.19: Error curve for 8 (top) and 4 (bottom) element TCAS at TC about 378.6" from nose at +10°.

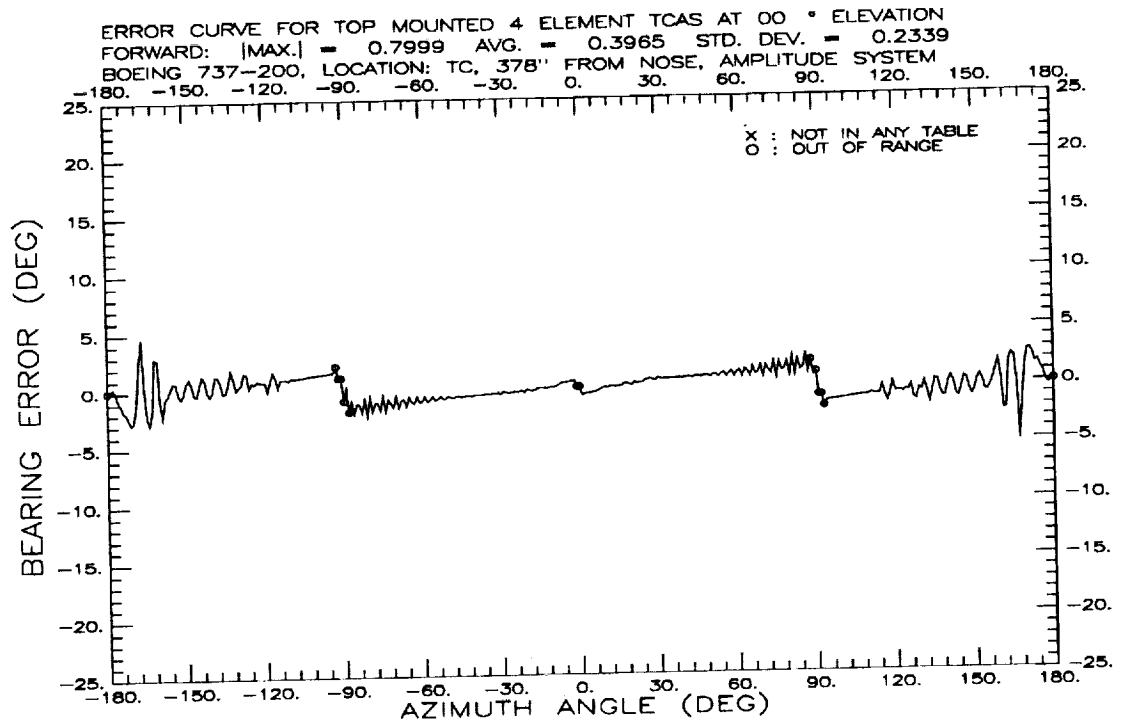
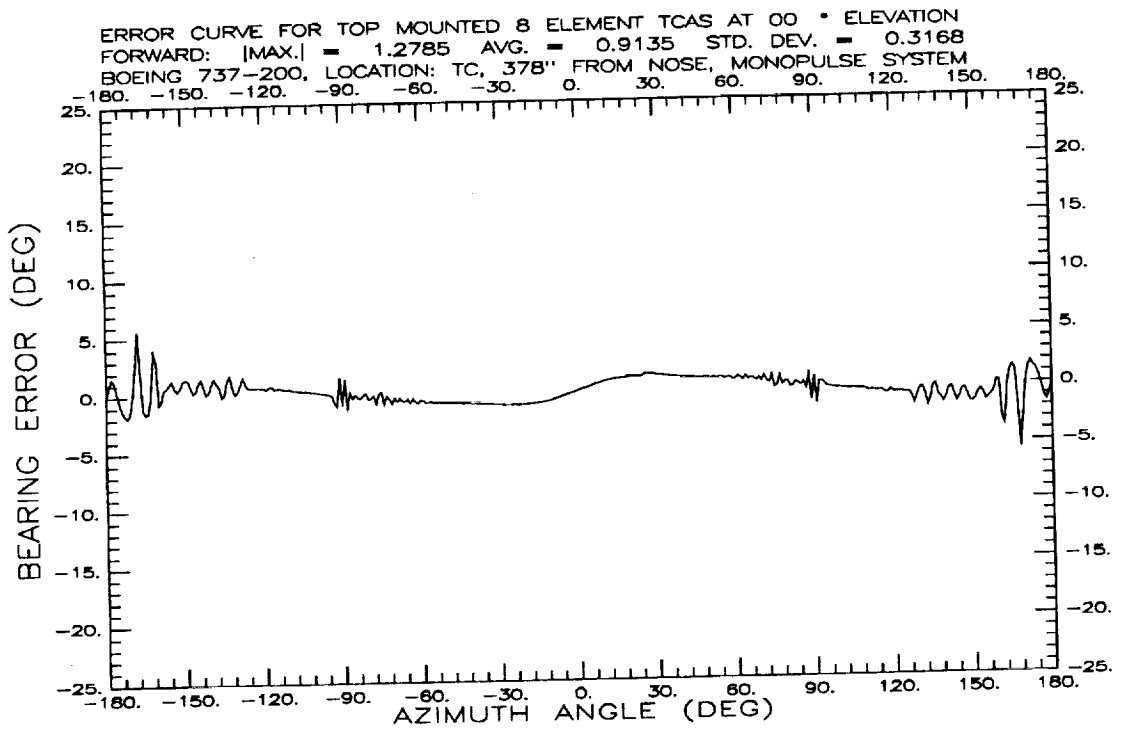


Figure 3.20: Error curve for 8 (top) and 4 (bottom) element TCAS at TC about 378.6" from nose at 0°.

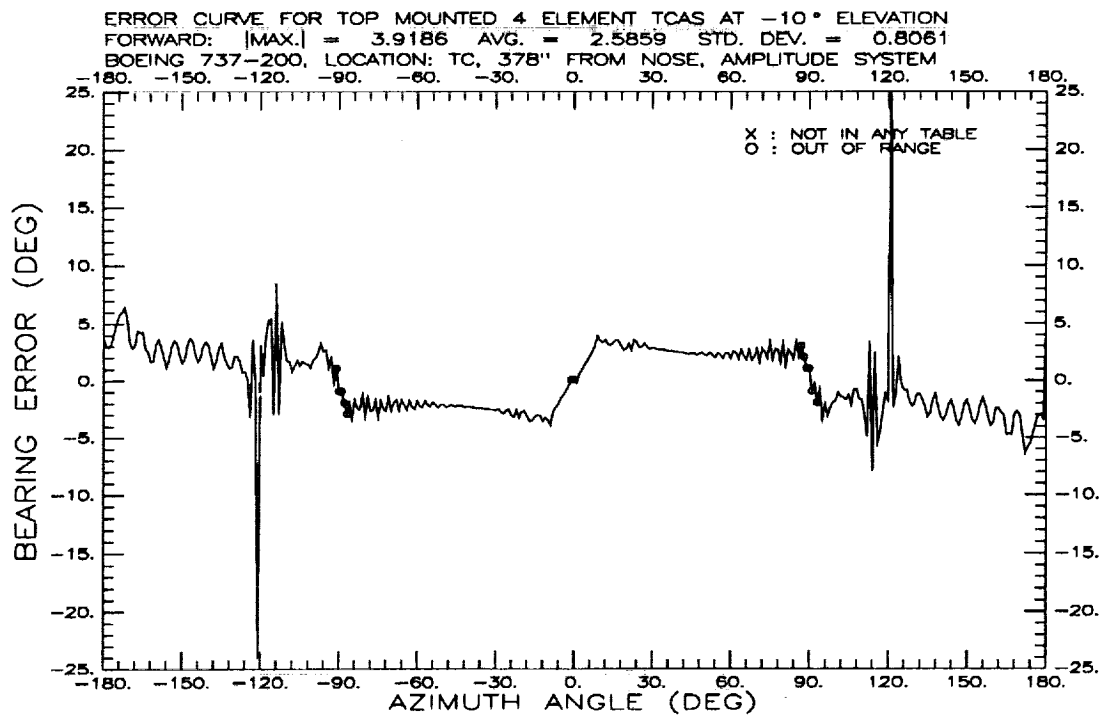
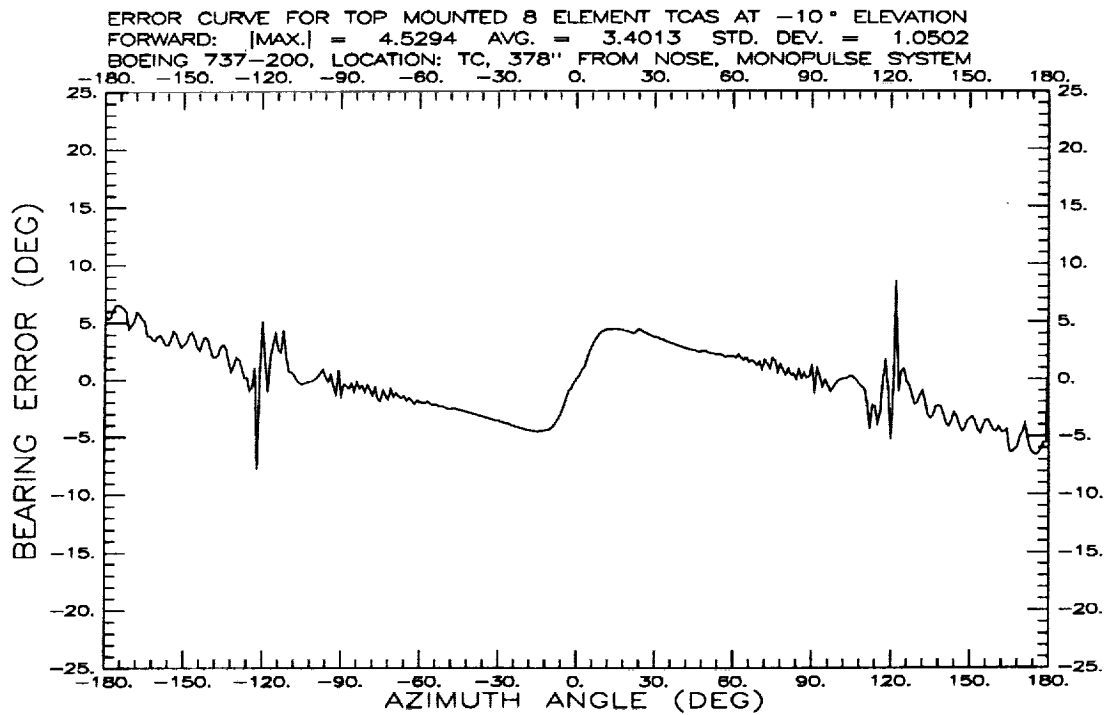


Figure 3.21: Error curve for 8 (top) and 4 (bottom) element TCAS at TC about 378.6" from nose at -10° .

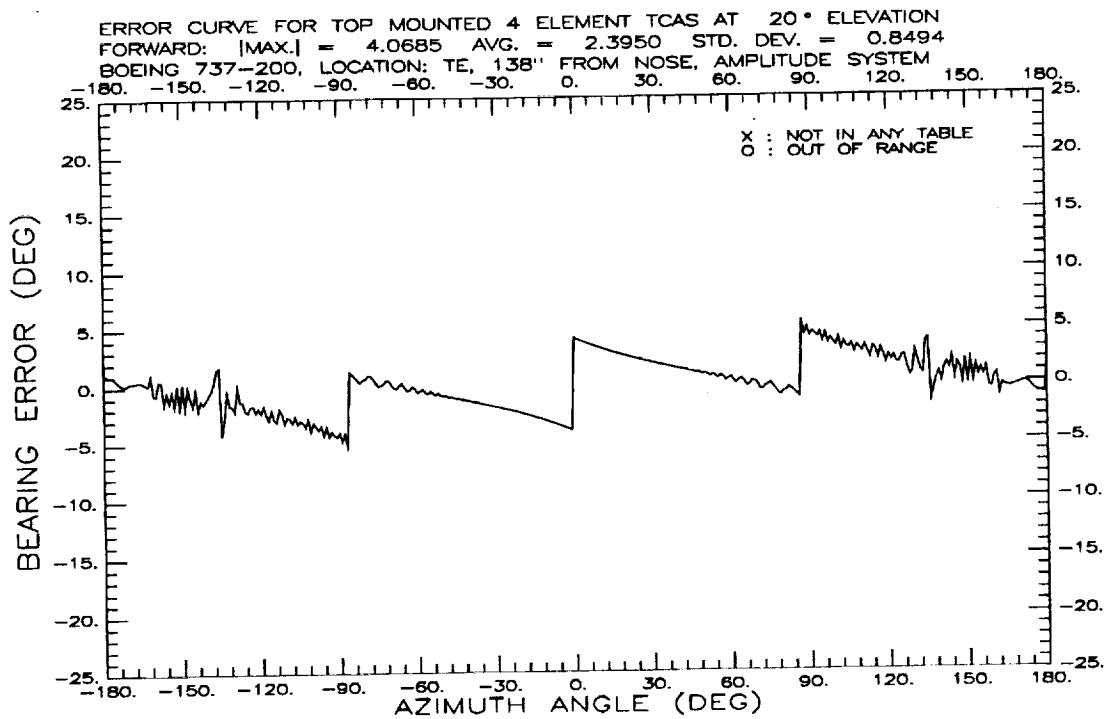
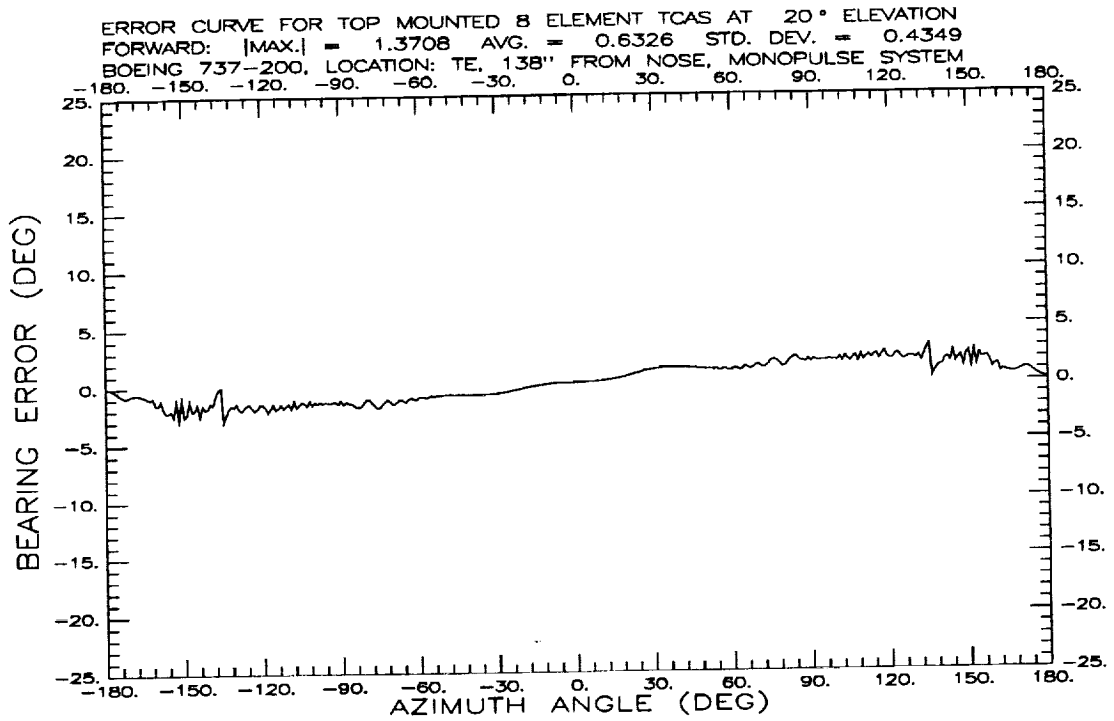


Figure 3.22: Error curve for 8 (top) and 4 (bottom) element TCAS at TE about 138.6" from nose at +20°.

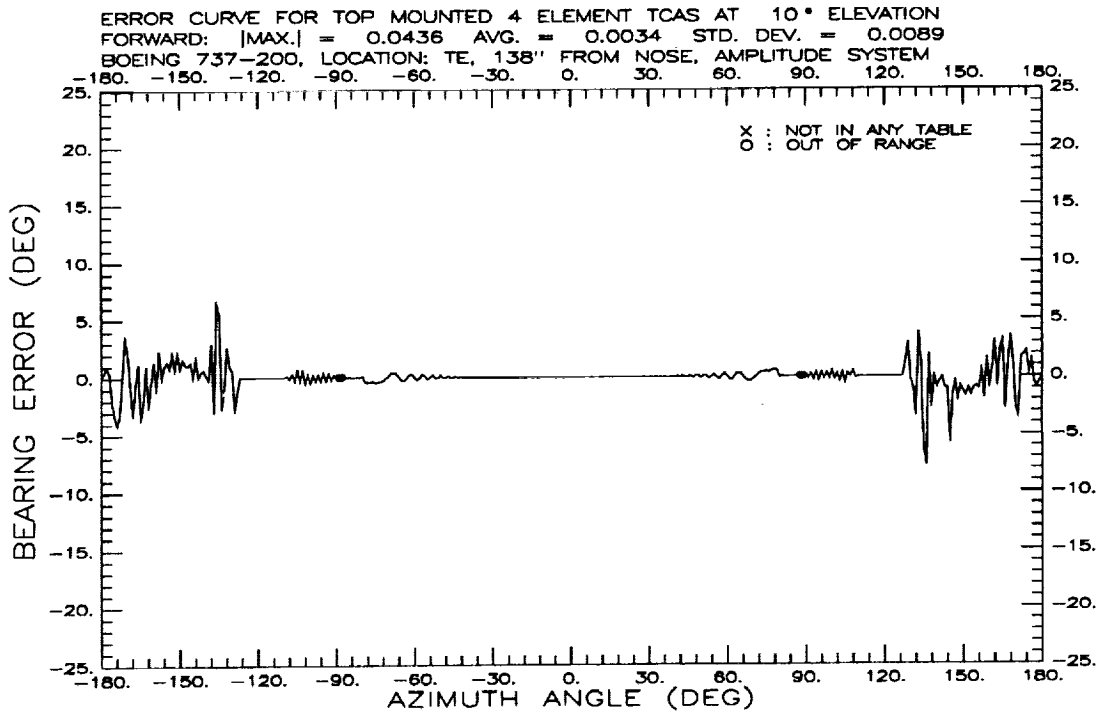
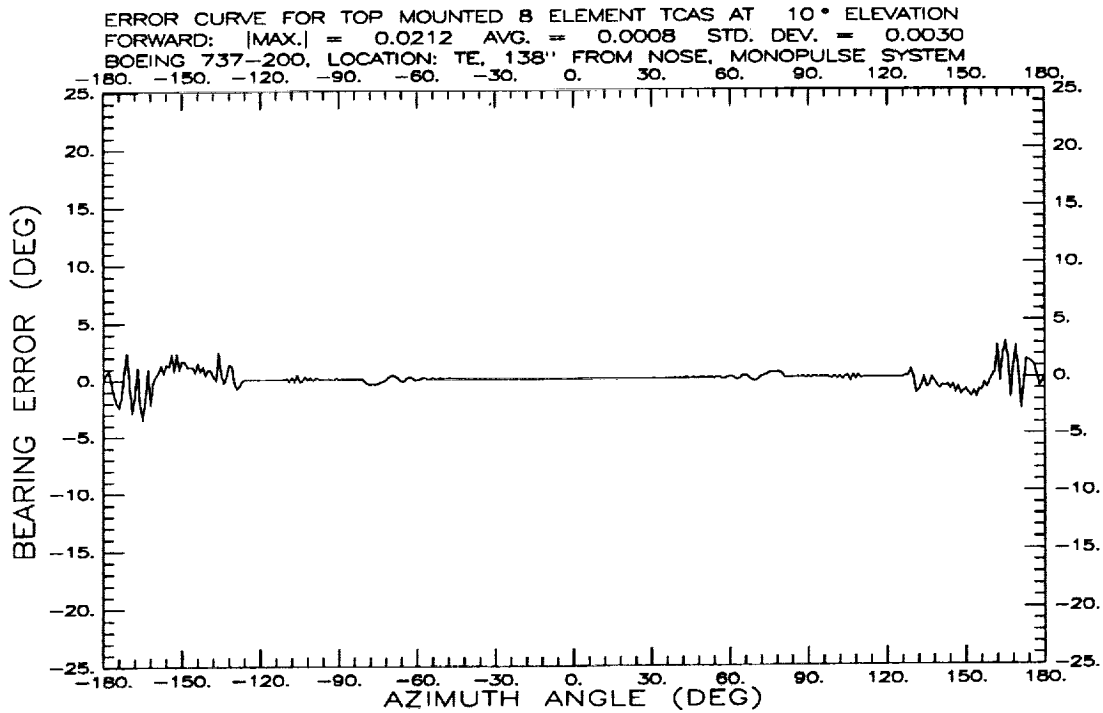


Figure 3.23: Error curve for 8 (top) and 4 (bottom) element TCAS at TE about 138.6" from nose at +10°.

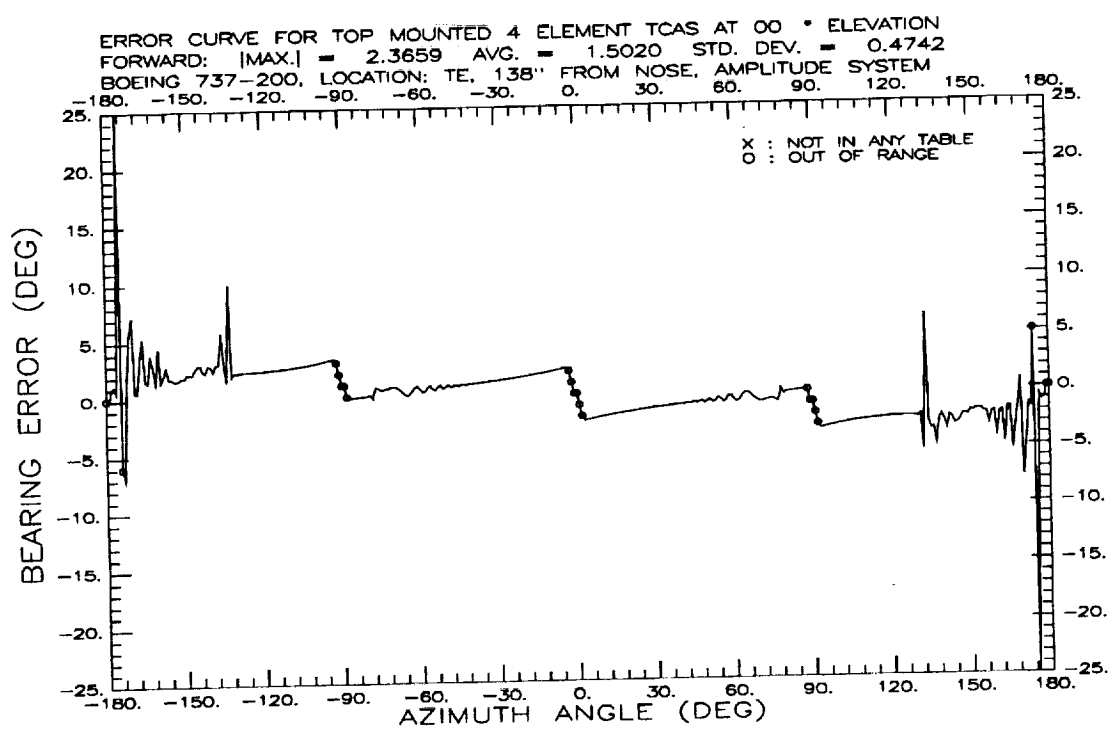
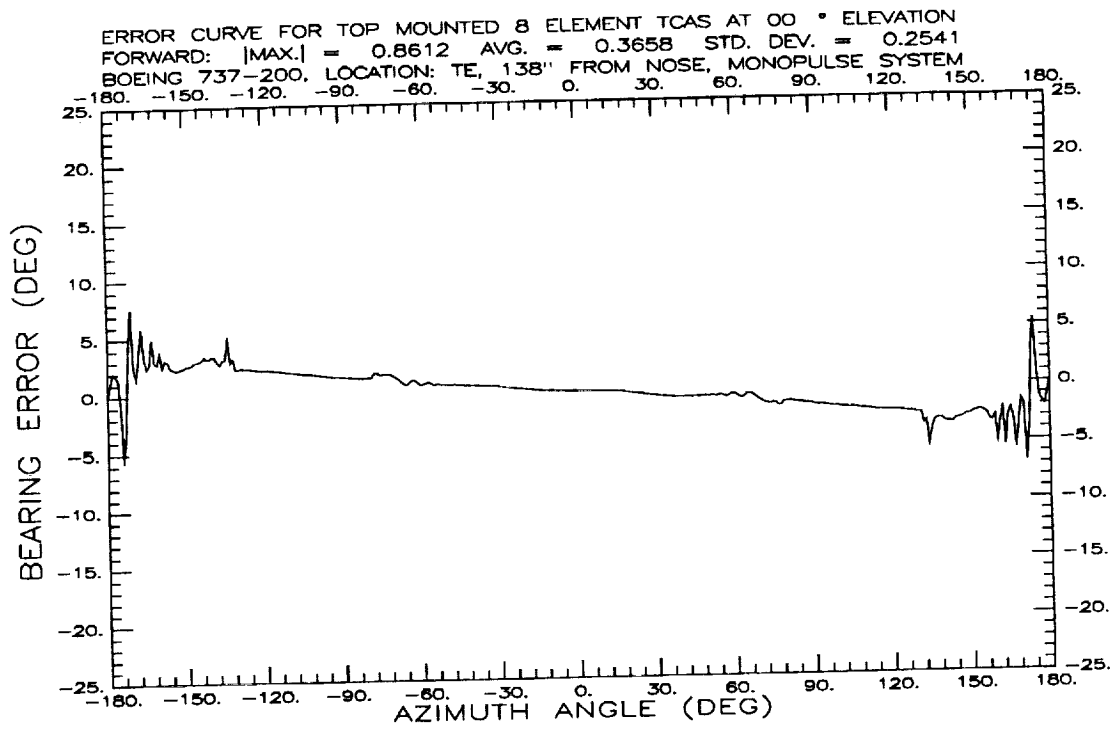


Figure 3.24: Error curve for 8 (top) and 4 (bottom) element TCAS at TE about 138.6" from nose at 0°.

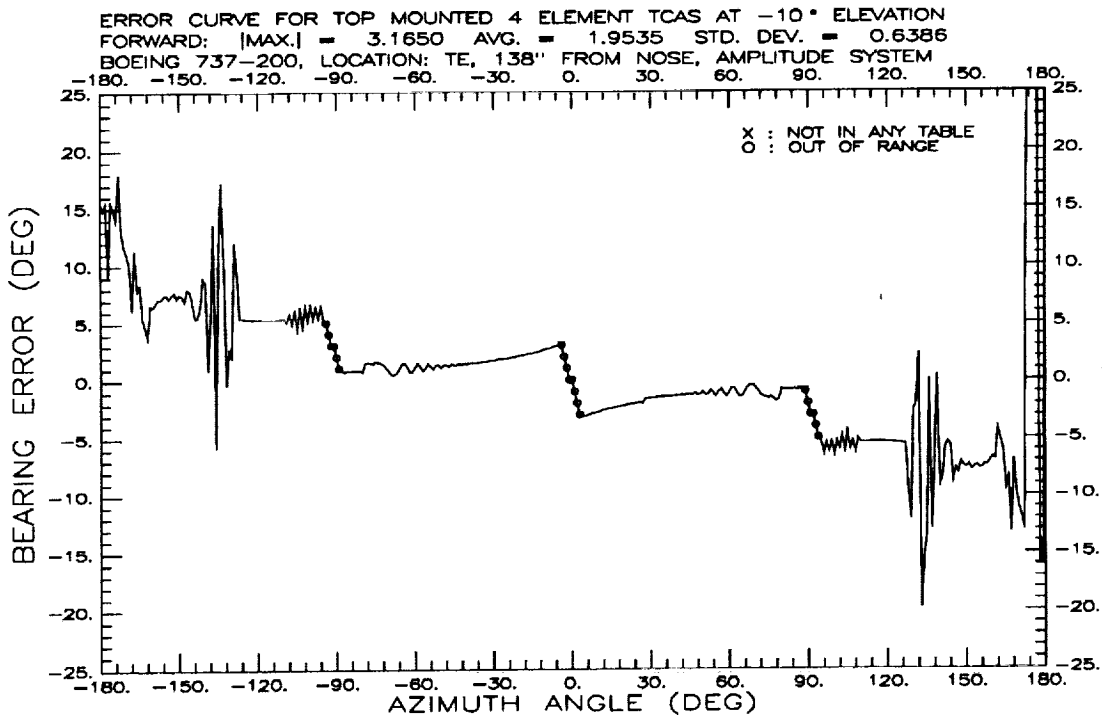
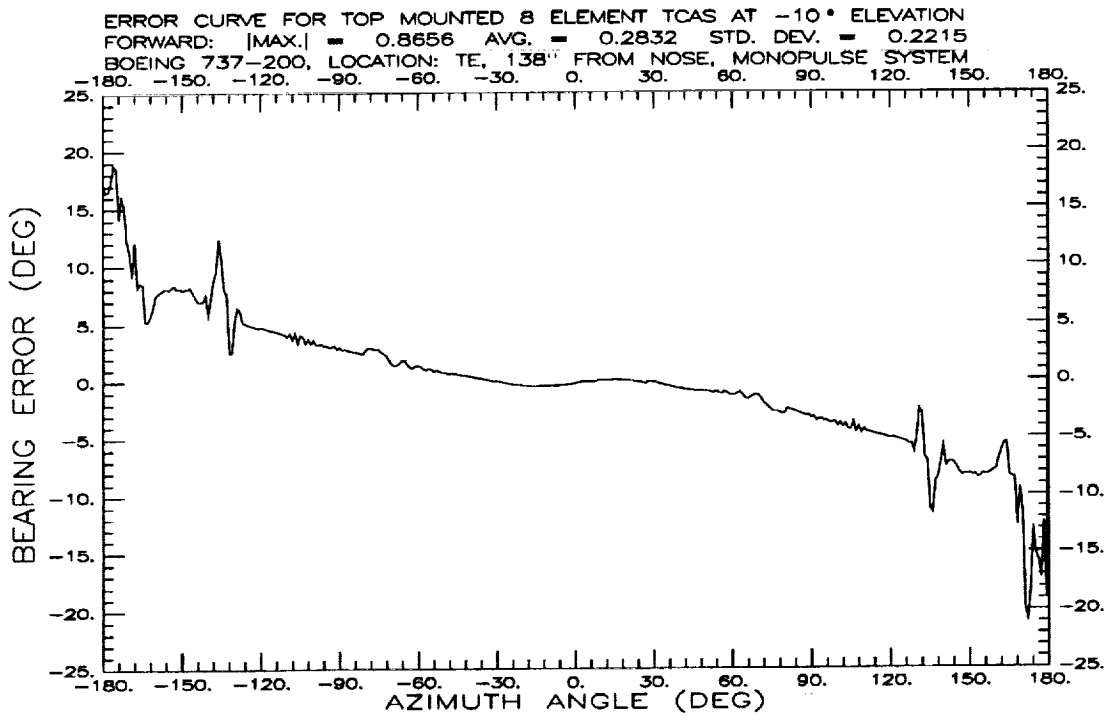


Figure 3.25: Error curve for 8 (top) and 4 (bottom) element TCAS at TE about 138.6" from nose at -10° .

Bibliography

- [1] "Enhanced TCAS II System Summary," Report No. BCD-TR-098, Bendix Communications Division, February 1984.
- [2] A.I. Sinsky, J.E. Reed and J. Fee, "Enhanced TCAS II Tracking Accuracy," AIAA/IEEE Digital Avionics Systems Conference Paper 84-2738-cp, December 1984.
- [3] R.G. Rojas, W.D. Burnside, P.H. Law and B. Grandchamp, "Simulation of the Enhanced Traffic Alert and Collision Avoidance System (TCAS II)," The Ohio State University ElectroScience Laboratory Technical Report 716199-3, generated under Grant No. NSG-1498, for NASA Langley Research Center, Hampton, Virginia, September 1985.
- [4] P.H. Law, W.D. Burnside and R.G. Rojas, "A Study of a Collision Avoidance System," The Ohio State University ElectroScience Laboratory Technical Report 716199-8, generated under Grant No. NSG-1498, for NASA, Langley Research Center, Hampton, Virginia, March 1986.
- [5] R.G. Rojas, W.D. Burnside, "Simulation of an Enhanced TCAS II System in Operation," The Ohio State University ElectroScience Laboratory Technical Report 716199-9, generated under Grant No. NSG-1498, for NASA, Langley Research Center, Hampton, Virginia, October 1987.
- [6] R.G. Rojas, Y.C. Chen, and W.D. Burnside, "Improved Computer Simulation of the TCAS III Circular Array Mounted on an Aircraft" The Ohio State University ElectroScience Laboratory Technical Report 716199-12, generated under Grant No. NSG-1498, for NASA, Langley Research Center, Hampton, Virginia, April 1989.

- [7] W.D. Burnside, J.J. Kin, B. Grandchamp, R.G. Rojas, and P.H. Law, "Airborne Antenna Radiation Pattern Code User's Manual," The Ohio State University ElectroScience Laboratory Technical Report 716199-4, generated for NASA, Langley Research Center, Hampton, Virginia, September 1985.
- [8] A. Altintas, P.H. Pathak, and W.D. Burnside, "Electromagnetic Scattering From a Class of Open-Ended Waveguide Discontinuities," The Ohio State University ElectroScience Laboratory Technical Report 716148-9, generated for NASA, Langley Research Center, Hampton, Virginia, March 1986.
- [9] R.J. Burkholder, C.W. Chuang, and P.H. Pathak, "Electromagnetic Fields Backscattered from an S-Shaped Inlet Cavity with an Absorber Coating on its Inner Walls," The Ohio State University ElectroScience Laboratory Technical Report 715723-2, generated for NASA, Lewis Research Center, Cleveland, Ohio, July 1987.
- [10] P.H. Law, R.J. Burkholder, and P.H. Pathak, "A Hybrid Asymptotic-Modal Analysis of the EM Scattering by an Open-Ended S-Shaped Rectangular Waveguide Cavity," The Ohio State University ElectroScience Laboratory Technical Report 719630-2, generated for NASA, Lewis Research Center, Cleveland, Ohio, December 1988.
- [11] C.A. Balanis, *Antenna Theory*, Harper & Row Publishers, Inc., 1982.
- [12] R. Sandholm, personal communication.

Appendix A

Statistics of Error Curves for 4 Element TCAS

The statistics of the error curves for a four element TCAS system employing amplitude comparison scheme are given below. Here, the azimuth space was divided into 4 equal quadrants, each covering 90°. For a top mounted antenna, the angular sectors covered are as given below in Table A.1:

Quadrant	Range (°)
Nose	-45 - 45
Left	45 - 135
Right	-45 - -135
Tail	-135 - -180 &135 - 179

Table A.1: Definition of sectors for computation of statistics for the error curves for top mounted antennas.

All the three locations studied in the report on Boeing 737-200 model for elevation angles 20°, 10°, 0°, and - 10° are presented. The statistics for the eight element TCAS III are given separately in Appendix B. These

statistics were compiled in each quadrant whose central direction is given by the beam heading. Even though the antenna is placed symmetrically and everything is symmetric in the aircraft structure, the statistics of left and right beams differ slightly due to numerical errors.

A.1 Location: TA

A.1.1 Elevation: 20°

quadrant	maximum abs. error	absolute average	standard deviation
nose	2.1399	1.3911	0.5266
left	5.6485	2.7949	1.7974
tail	14.0032	3.0247	2.9121
right	5.5592	2.7693	1.7733

A.1.2 Elevation: 10°

quadrant	maximum abs. error	absolute average	standard deviation
nose	0.8637	0.1740	0.2401
left	8.6480	0.7447	1.1490
tail	6.7940	2.3327	1.7162
right	6.8816	0.7022	0.9928

A.1.3 Elevation: 0°

quadrant	maximum abs. error	absolute average	standard deviation
nose	1.5938	0.7438	0.3345
left	2.3974	1.0772	0.5881
tail	5.5305	1.7485	1.7144
right	2.4208	1.0801	0.5731

A.1.4 Elevation: -10°

quadrant	maximum abs. error	absolute average	standard deviation
nose	6.4603	4.6556	1.0581
left	6.7549	2.0409	1.2004
tail	7.2708	2.4270	1.8210
right	6.6367	1.9790	1.2053

A.2 Location: TC

A.2.1 Elevation: 20°

quadrant	maximum abs. error	absolute average	standard deviation
nose	2.4655	1.0420	0.7426
left	3.6667	1.4255	0.8578
tail	16.3032	2.9870	3.3225
right	3.6356	1.4219	0.8613

A.2.2 Elevation: 10°

quadrant	maximum abs. error	absolute average	standard deviation
nose	0.1062	0.0326	0.0228
left	8.2518	0.6527	1.0529
tail	3.6842	1.3527	0.9785
right	6.7313	0.6506	0.9319

A.2.3 Elevation: 0°

quadrant	maximum abs. error	absolute average	standard deviation
nose	0.7999	0.3965	0.2339
left	2.4376	1.0792	0.4662
tail	5.2000	1.1091	1.0327
right	2.3412	1.0558	0.4715

A.2.4 Elevation: -10°

quadrant	maximum abs. error	absolute average	standard deviation
nose	3.9186	2.5859	0.8061
left	30.1583	2.5023	3.1216
tail	6.4250	3.1857	1.1930
right	24.1049	2.4468	2.5799

A.3 Location: TE

A.3.1 Elevation: 20°

quadrant	maximum abs. error	absolute average	standard deviation
nose	4.0685	2.3950	0.8494
left	5.4521	1.8278	1.4502
tail	4.2690	0.8650	0.7366
right	5.2660	1.8100	1.4454

A.3.2 Elevation: 10°

quadrant	maximum abs. error	absolute average	standard deviation
nose	0.0436	0.0034	0.0089
left	6.3941	0.3678	0.8941
tail	7.7472	1.7269	1.5266
right	5.4898	0.3404	0.7521

A.3.3 Elevation: 0°

quadrant	maximum abs. error	absolute average	standard deviation
nose	2.3659	1.5020	0.4742
left	6.4782	1.6970	1.2955
tail	28.3948	3.2146	4.0513
right	9.9965	1.6599	1.4137

A.3.4 Elevation: -10°

quadrant	maximum abs. error	absolute average	standard deviation
nose	3.1650	1.9535	0.6386
left	19.7826	3.5648	3.3920
tail	66.8649	10.9870	11.0476
right	17.2241	3.4288	2.9966

Appendix B

Statistics of Error Curves for 8 Element TCAS III

The statistics of the error curves for the 8 element TCAS system employing monopulse detection scheme are given below. All the three locations studied in the report on Boeing 737-200 model for elevation angles 20° , 10° , 0° , and -10° are presented. The statistics for the four element TCAS are given separately in Appendix A. These statistics were compiled in each quadrant whose central direction is given by the beam heading as given in Table A.1.

B.1 Location: TA

B.1.1 Elevation: 20°

quadrant	maximum abs. error	absolute average	standard deviation
nose	2.8784	1.1011	1.0214
left	4.0674	1.1479	1.2782
tail	4.8954	1.9619	1.1515
right	4.2650	1.2296	1.3324

B.1.2 Elevation: 10°

quadrant	maximum abs. error	absolute average	standard deviation
nose	0.9059	0.2073	0.2675
left	1.3693	0.4475	0.3514
tail	5.7911	2.0495	1.4485
right	1.5274	0.4621	0.3821

B.1.3 Elevation: 0°

quadrant	maximum abs. error	absolute average	standard deviation
nose	2.1358	1.3763	0.4512
left	1.6834	0.6833	0.5298
tail	5.3393	1.5297	1.3688
right	1.7413	0.6702	0.5556

B.1.4 Elevation: -10°

quadrant	maximum abs. error	absolute average	standard deviation
nose	7.2120	5.5706	1.1251
left	5.2918	1.6028	1.1102
tail	5.9656	3.0817	1.1004
right	6.9273	1.6184	1.2276

B.2 Location: TC

B.2.1 Elevation: 20°

quadrant	maximum abs. error	absolute average	standard deviation
nose	0.6004	0.2802	0.1597
left	2.0376	0.4949	0.3501
tail	6.4823	1.6089	1.5227
right	2.5270	0.6106	0.4243

B.2.2 Elevation: 10°

quadrant	maximum abs. error	absolute average	standard deviation
nose	0.0210	0.0015	0.0036
left	2.4957	0.4709	0.5719
tail	3.5620	1.1568	0.8615
right	2.8144	0.4628	0.5691

B.2.3 Elevation: 0°

quadrant	maximum abs. error	absolute average	standard deviation
nose	1.2785	0.9135	0.3168
left	1.9035	0.6009	0.3613
tail	5.6623	1.1692	1.0139
right	1.6856	0.5987	0.3772

B.2.4 Elevation: -10°

quadrant	maximum abs. error	absolute average	standard deviation
nose	4.5294	3.4013	1.0502
left	8.4830	1.4599	1.2745
tail	6.5789	4.2795	1.2445
right	7.7653	1.4813	1.1987

B.3 Location: TE

B.3.1 Elevation: 20°

quadrant	maximum abs. error	absolute average	standard deviation
nose	1.3708	0.6326	0.4349
left	3.1210	1.7626	0.4419
tail	3.1210	1.2723	0.7713
right	3.0283	1.4463	0.3861

B.3.2 Elevation: 10°

quadrant	maximum abs. error	absolute average	standard deviation
nose	0.0212	0.0008	0.0030
left	1.3727	0.1395	0.2420
tail	3.3559	1.1726	0.7327
right	1.3450	0.1446	0.2292

B.3.3 Elevation: 0°

quadrant	maximum abs. error	absolute average	standard deviation
nose	0.8612	0.3658	0.2541
left	5.2446	1.7227	0.7893
tail	7.5368	3.0249	1.2081
right	4.7609	1.5317	0.6981

B.3.4 Elevation: -10°

quadrant	maximum abs. error	absolute average	standard deviation
nose	0.8656	0.2832	0.2215
left	11.2865	3.2372	1.8211
tail	20.8642	9.9055	3.8429
right	10.5944	3.0594	1.7933

